Renewable Energy 256 (2026) 124609

Contents lists available at ScienceDirect

Renewable Energy

journal homepage: www.elsevier.com/locate/renene

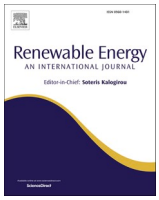

Off-grid shore-to-ship power system optimization with a hydrogen-in-loop buffering scheme driven by hydrokinetic wave-wind energy

Hadi Taghavifar [a,b,*], Chiara Bordin [c], Hao Chen [d], Anthony Paul Roskilly [a]

[a] Department of Engineering, Durham University, Durham, DH1 3LE, UK
[b] Department of Technology and Safety, UiT the Arctic University of Norway, Tromsø, Norway
[c] Department of Computer Science, UiT the Arctic University of Norway, Tromsø, Norway
[d] IEBIS Department of High-tech Business and Entrepreneurship, University of Twente, the Netherlands

ARTICLE INFO

Keywords:
Arctic energy
Game theory optimization
Hydrogen-in-loop (H2iL)
Renewable energy system
RSM virtual meta-models

ABSTRACT

The environmentally vulnerable Arctic's harsh climate and remote geography demand innovative green energy solutions. This study introduces a hybrid off-grid system that integrates wave and wind energy with hydrogen-electricity conversion technologies. Designed to power cruise ships at berth, fuel-cell hybrid electric vehicles, and residential heating, the system tackles the challenge of energy variability through dual optimization schemes. External optimization identifies a cost-effective architecture, achieving a net present cost of $1.1M and a levelized hydrogen cost of $20.1/kg without a fuel cell. Internal optimizations, employing multi-objective game theory and HYBRID algorithms, further improve performance, reducing the net present cost to $666K with a levelized hydrogen cost of $13.74/kg (game theory) and $729K with a levelized hydrogen of $15.63/kg (HYBRID). A key innovation is hydrokinetic turbines, which streamline the design by cutting cumulative cash flow requirements by $470K, from $1.85M to $1.38M. This approach prioritizes intelligent energy management, shifting reliance from variable wind and wave inputs to optimized electrolyzer and battery operations. These results underscore the feasibility of cost-effective and scalable renewable energy systems and provide a compelling blueprint for addressing energy challenges in remote and resource-constrained environments.

1. Introduction

Arctic, with its vast natural resources, holds significant potential for renewable energy utilization but is hindered by distinct challenges [1]. Its off-grid nature limits access to centralized energy networks [2], while the cold climate intensifies energy demands for heating [3]. Furthermore, the region relies heavily on intermittent energy sources, such as wind and wave power, which are inherently variable and require robust storage and management systems to ensure reliability [4]. Leveraging DSS tools to address these challenges is critical for realizing sustainable energy solutions tailored to the unique context of Northern Norway [5].

The paper addresses the critical need for optimized hybrid energy systems capable of supporting cold ironing, providing shoreside power to docked ships, and catering to multi-load applications such as residential heating and fueling fuel-cell hybrid electric vehicles (FCHEVs). Cold ironing refers to the process of providing shore-based electrical power to ships while they are docked, allowing them to shut down their onboard engines and reduce emissions.

Cold ironing is very challenging in remote and off-grid regions like Northern Norway [6], where reliance on intermittent renewable energy sources such as wind and wave intensifies the need for efficient energy storage and management solutions. In the case of wind, this intermittency arises from both policy and planning challenges for offshore wind deployment in Norway [7] and the operational variability and ramping characteristics of wind power output [8], which complicate supply-demand balancing and grid reliability. Similarly, wave energy has variability and intermittency due to changing sea-state conditions and weather patterns. This also requires in-depth forecasting and integration strategies to ensure reliable power delivery [9]. In this broad context, hydrogen emerges as a pivotal clean energy carrier. Indeed, its underground storage potential has been evaluated in Norway's depleted oil and gas fields [10], and national strategies increasingly recognize hydrogen's role in future low-carbon export pathways despite delays in the broader energy transition [11]. All in all, hydrogen offers a flexible and sustainable pathway for energy storage and conversion [20].

By leveraging hydrogen's ability to store excess electricity and

* Corresponding author. Department of Engineering, Durham University, Durham DH1 3LE, UK.
E-mail addresses: haditaghavifar@yahoo.com, hadi.taghavifar@durham.ac.uk (H. Taghavifar).

https://doi.org/10.1016/j.renene.2025.124609
Received 7 April 2025; Received in revised form 28 September 2025; Accepted 11 October 2025
Available online 13 October 2025

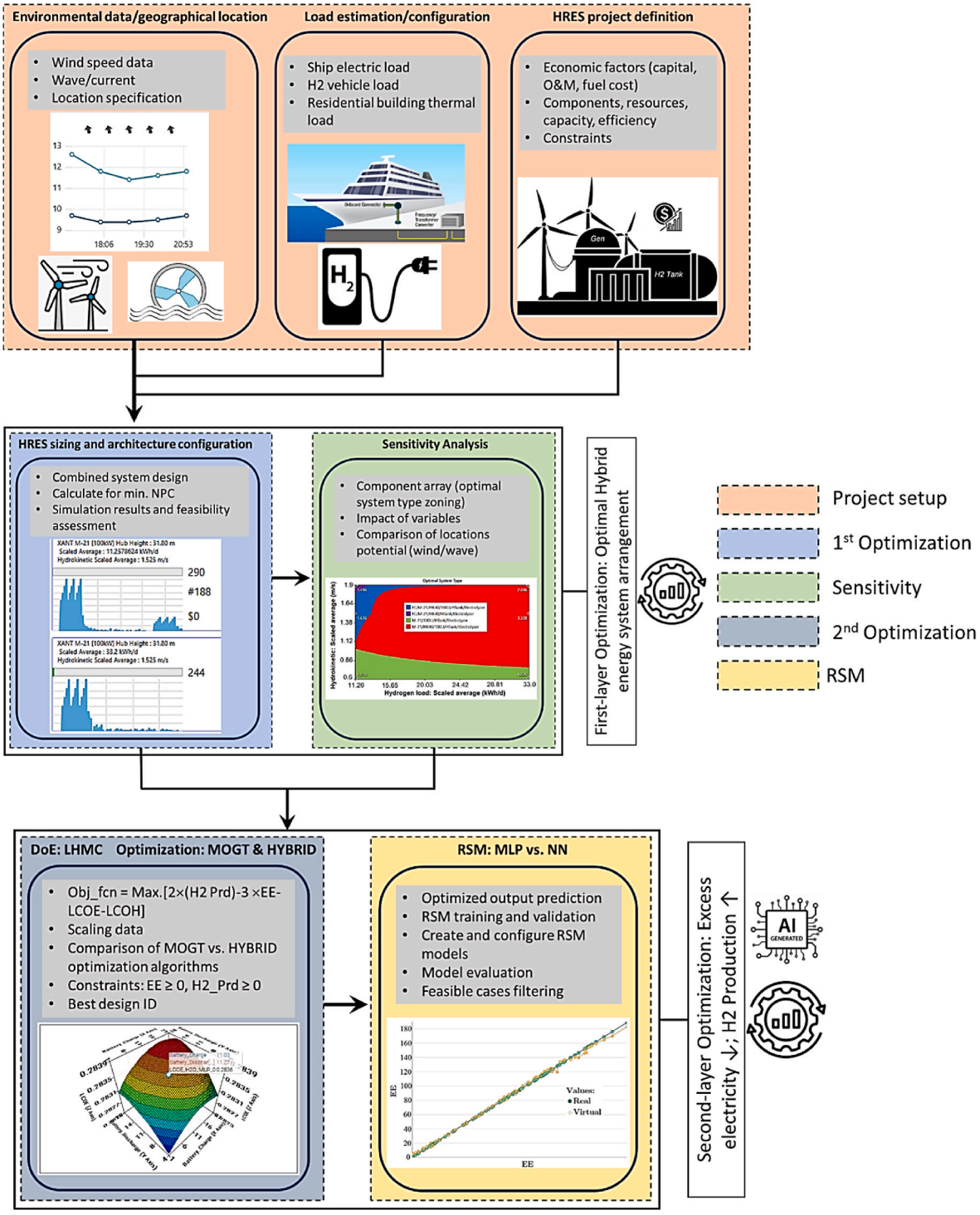

Fig. 1. The schematic workflow representation of 1- hybrid off-grid renewable energy system designed based on a case-specific wave-wind sources in north-Norway for cogeneration of hydrogen-electricity meeting cold-ironing, hydrogen station, and the thermal load; 2- first-step genetic algorithm optimization; 3- second-step optimization with RSM meta-models.

provide on-demand energy through fuel cells, this research seeks to develop AI-optimized configurations that integrate hydrogen into hybrid systems, addressing energy variability while minimizing costs and environmental impacts.

Fig. 1 illustrates the schematic workflow of the proposed hybrid off-grid renewable energy system, tailored to Arctic-specific energy challenges and resources. The system is designed to harness wave and wind energy for the cogeneration of hydrogen and electricity, serving three distinct applications: cold ironing for docked cruise ships, fueling hydrogen stations for fuel-cell hybrid electric vehicles (FCHEVs), and supplying thermal loads for residential heating. The workflow integrates a two-step optimization process. In the first step, a genetic algorithm identifies the optimal configuration of system components, including electrolyzers, hydrogen storage, and renewable energy inputs. This is followed by a second-step optimization using Response Surface Methodology (RSM) meta-models to fine-tune energy flow strategies, aiming

to minimize excess electricity, reduce costs, and maximize hydrogen production. The figure encapsulates the structured approach to designing and optimizing a hybrid system that addresses the unique energy demands of Northern Norway.

The schematic workflow (Fig. 1) highlights the systematic methodology adopted, ensuring that the system is robust, efficient, and capable of meeting the diverse energy demands of cold ironing, hydrogen fueling, and residential heating. This research sets the stage for developing scalable solutions that can serve as models for other remote and off-grid regions.

2. Literature review

Cold ironing, or providing shoreside power to docked ships, is an increasingly important solution to reduce emissions and environmental impact from ships at port. Several studies have explored cold ironing systems that integrate renewable energy sources, particularly wind and solar power, to meet the high electricity demands of cruise ships while minimizing reliance on fossil fuels. For example, one study proposes a renewable-powered cold ironing system for the Port of Barcelona based entirely on wind and solar energy sources [12], while another assesses the environmental and economic performance of hybrid systems combining photovoltaics, batteries, fuel cells, and ammonia-based hydrogen production [13]. Recent advancements have also highlighted the potential of combining renewable energy sources with hydrogen technologies to create hybrid systems [14]. These hybrid systems often integrate wind and wave energy with hydrogen storage and fuel cells, providing a flexible and sustainable approach to energy generation and storage [15]. The use of hydrogen allows for efficient storage of excess renewable energy [16], which can be converted back into electricity or used for other applications, such as powering fuel-cell hybrid electric vehicles (FCHEVs) [17] or meeting thermal loads [18]. In Northern Norway, where energy demands are high and renewable resources are plentiful but variable, this is particularly important. Studies have looked at the wider role of hydrogen in Norway's national energy transition strategies [19], the techno-economic viability of renewable-based hybrid systems for electrifying remote Norwegian islands using hydrogen and battery storage [20], and the operational performance of an autonomous wind-hydrogen demonstration system on the island of Utsira, which has provided insights into design and efficiency improvements for off-grid applications [21]. In early hybrid energy systems, such as Utsira [21,22], wind-to-hydrogen buffering is implemented for a small-scale community island. However, this system configuration is limited to residential electricity in coastal settings, without considering the multi-sector energy demands and challenges associated with cold climates in Arctic ports.

Our research fills the gap by proposing a new buffering concept (H2iL) that integrates residential, marine, and hydrogen refueling (multi-sector integration) within a multi-tier optimization framework to address the resilience requirement in the cold-region ports with a layered storage system and bidirectional energy flow.

Hydrogen plays a crucial role in enhancing renewable energy systems by acting as a versatile energy carrier [23]. Electrolyzers, which produce hydrogen from water using electricity, are paired with storage tanks and fuel cells to create efficient, sustainable solutions [24].

Hydrogen can smooth out changes in energy from sources that are intermittent, like wind and solar, and make it possible to store energy in the long term. This is extensively discussed in reviews analyzing hydrogen's potential as both an energy carrier and storage medium [25] and highlighting the challenges, opportunities, and decentralization potential of hydrogen systems powered by renewables [26]. Northern Norway is rich in renewable energy resources, particularly wind and wave energy, thanks to its geographical location along the Arctic Circle [27]. The region experiences strong and consistent winds, making it ideal for wind power generation [28]. Similarly, wave energy holds significant potential, driven by the region's exposure to powerful ocean currents [29]. Hydrokinetic turbines, which harness energy from water currents, are increasingly being explored to complement these resources. These turbines offer a stable, low-maintenance energy solution and are well-suited to Northern Norway's challenging, off-grid conditions [30].

AI-driven optimization techniques, such as game theory and hybrid methods, have shown great promise in the design of renewable energy systems [31]. These techniques can handle the complex and multi-faceted nature of hybrid energy systems, where multiple energy sources and storage solutions must be integrated efficiently. Multi-objective optimization, often using methods like genetic algorithms or meta-models, helps to balance competing goals, such as minimizing costs, maximizing energy production, and ensuring system reliability.

Unlike conventional hydrogen buffering schemes that typically operate as one-way seasonal backup, the proposed Hydrogen-in-Loop (H2iL) method proposes a multiloop, energy architecture that integrates battery, electrolyzer, and fuel cell operation in a bidirectional energy flow platform. This configuration optimizes energy flows across daily and seasonal cycles, allowing for bidirectional energy exchange under Arctic constraints. Compared to other hybrid H_2 systems [32] which hybridize the battery and hydrogen for short- and long-term buffering, the H2iL specifically adapts to cold-region limitations by preserving battery SOC and deferring storage losses over the seasonal period.

3. Innovation and key contributions

Soft linking is a valuable methodological contribution because it allows for the seamless integration of multiple tools and models that would otherwise operate independently. This approach enhances the accuracy of system performance evaluations and provides a dynamic solution that can adjust to various objectives, such as minimizing costs and maximizing energy production. By linking tools in a modular fashion, the methodology enables more comprehensive and adaptable energy system analysis.

The significant contributions of the study are as follows:

1. This study develops an off-grid hybrid system combining wave and wind energy with hydrogen-electricity conversion to meet diverse demands, including maritime cold ironing, hydrogen refueling, and residential heating. This system provides a unified solution for renewable energy applications.
2. Employing a two-tier optimization framework, the system integrates architectural design with energy flow management, optimizing excess electricity, cost efficiency, and hydrogen production for enhanced system performance.
3. The integration of hydrokinetic turbines leverages wave energy, reducing dependency on conventional components while enhancing flexibility and showcasing the untapped potential of hydrokinetic resources.
4. Designed for the Remote Arctic's unique challenges, the system's modular and adaptive design addresses energy variability and infrastructure limitations, offering a replicable model for isolated and resource-constrained environments.
5. Novel Hydrogen-in-Loop Architecture: Introduce an innovative system design for hybrid renewable energy, optimizing hydrogen production and energy flow.
6. Soft Linking of Multiple Tools: Combine multiple energy hybridizing analysis and decision-making platforms for internal optimization, game theory implementation, and hybrid optimization, creating a flexible, efficient workflow.
7. Multi-Objective Optimization: Use a game-theory-based hybrid optimization approach to balance energy production, costs, and efficiency, addressing unique challenges in Northern Norway's cold-climate, off-grid settings.

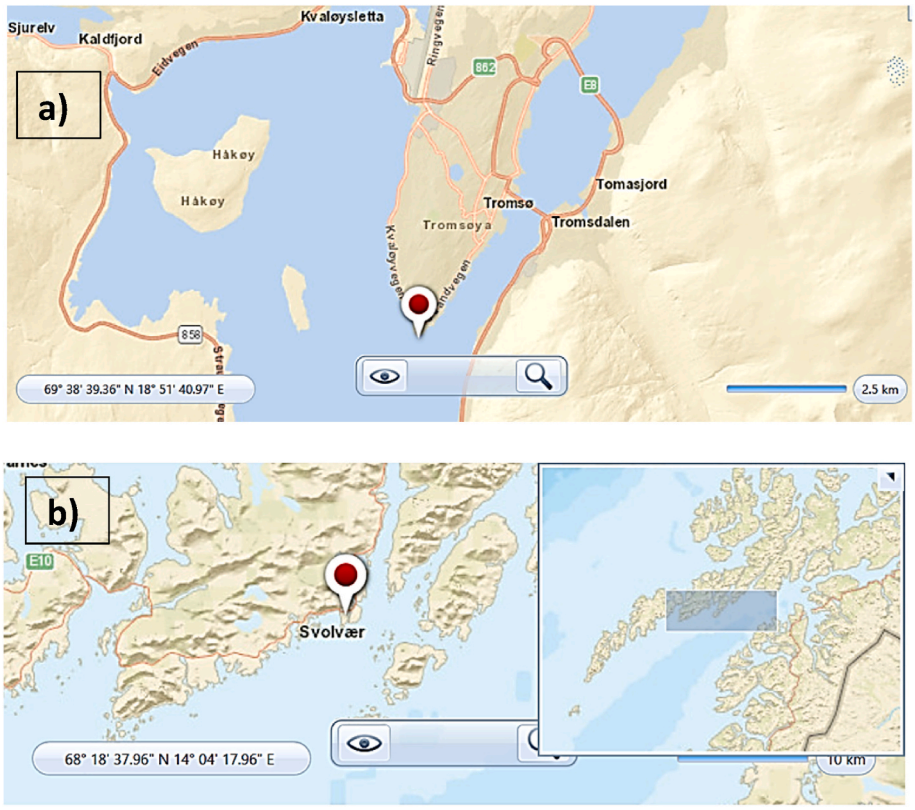

Fig. 2. The hybrid off-grid system deployment locations in Northern Norway, a) Tromso, b) Svolvær archipelago in Lofoten.

4. Methodology

4.1. Site characteristics and load profiles

Wind and hydrokinetic sources provide intermittent renewable energy for a microgrid system. In the Arctic region, extensive shorelines exist with a good capacity for wave kinetics and energy harvesting. Additionally, in this region, wind energy is powerful and shows synergy to be coupled with wave energy. This means that in some seasons, there is an abundance of energy supply, while in other seasons, there are energy shortages in a hybrid off-grid system based on hydrokinetic turbine–wind turbine (HKT-WT) operation. The first solution is to use energy storage (battery) and energy carriers such as hydrogen to have a sustainable energy paradigm. The second solution that is addressed here is the minimization of excess electricity while maintaining the hydrogen production rate and considering the techno-economic schemes by adopting optimization schedulers. The main site of investigation is in the Tromsø region, where cruise ships are docked in a harboring state, making it an ideal location to evaluate cold ironing with smart renewable energy sources benchmarking and future hydrogen fueling plans. The secondary location in the northern area is at the Lofoten archipelago, which has significantly better wind and wave energy potential, and its average wind and wave profiles will be used in the sensitivity analysis. The topographic locations of the microgrid system utilization sites are illustrated in Fig. 2 for Tromsø, the main investigation site, and Svolvær in Lofoten, which serves as a case study for wind and water kinetic potential. The selection of both Tromsø and the Lofoten archipelago is based on technical, geographic, and policy-driven considerations relevant to Arctic energy transition strategies. The site selection for this study is based on the following criteria:

- These locations demonstrate high potential for renewable energy, offering rich wave and wind energy resources.

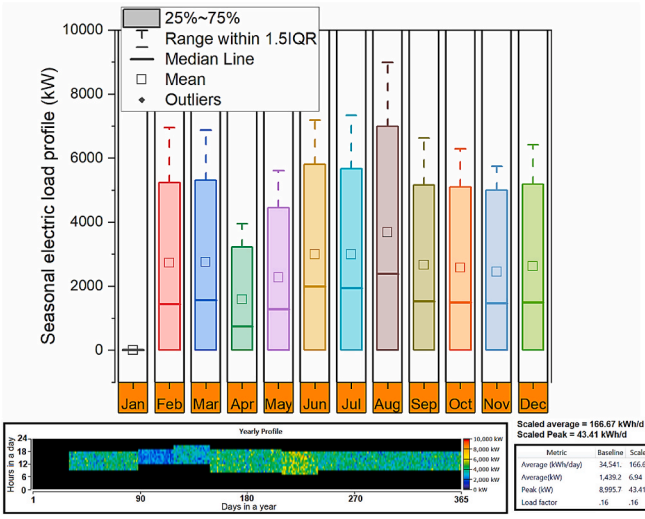

Fig. 3. The electric load profile based on the ship's electric power requirement in Tromso.

- There is limited grid connectivity, particularly in remote communities facing harsh environmental conditions.
- From maritime and hydrogen policy, the selected sites are in the strategic regions known for testbeds of the green shipping corridor and logistics hub.

Regarding contrasting Tromsø and Lofoten, Tromsø has a higher average wind profile with lower wave energy intensity, which makes it a good option for electrolyzer efficiency optimization.

The primary electric load is designated for the cruise ship's (CS) shore power at port. To this end, a frequency transformer connection is

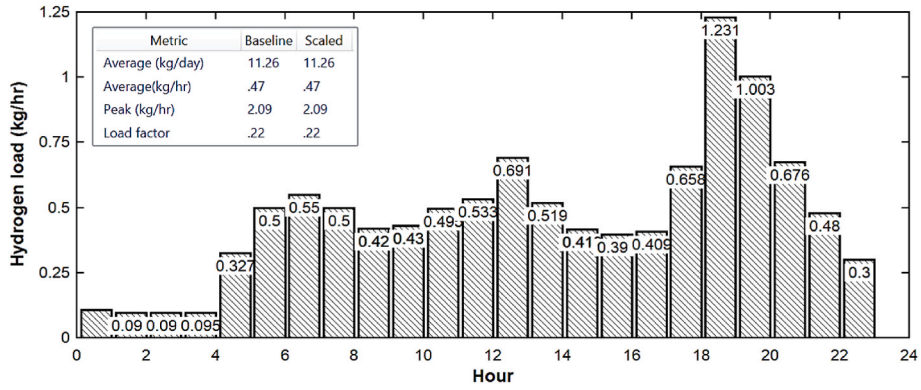

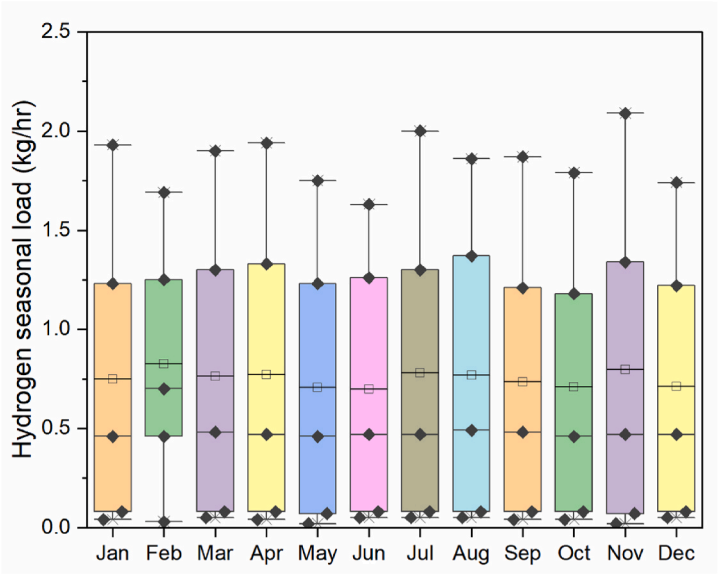

Fig. 4. Hydrogen daily and seasonal loads.

used, and the power is distributed to different components via a control panel. Tromso harbor is still not equipped with offshore power infrastructure to electrify the tourist CSs [33]. The electricity demand for a docked CS ranges from 4.3 MW to 11.1 MW with a variety of passenger capacity and shore power connection possibilities [34]. For instance, a case in point is the Koningsdam ship with a 2650-passenger capacity and equipped with a shore power connection, which requires 4.7–5.5 MW power while harbored at Kristiansand port. Based on the statistics [33, 35], a typical CS needs an average of 5 MW of electric load in hoteling mode. The load distribution data for different ship sizes and during other months are collected and used to estimate the electric load for the primary electric load, and the result of the distribution is shown in Fig. 3. As observed, no CS is visiting or docked at the port, and there is no electric load requirement in January. The seasonal and annual electric load range, along with statistical measures, is demonstrated and must be supplied through renewable energy sources. It is expected that the system will be responsive for meeting electric energy demands within the 25–75 % typical range and be prepared to handle the extreme range within 1.5 times the interquartile range (IQR).

Hydrogen demand is repurposed for H_2 fueling station for powering of fuel cell electric vehicle (FCEV) with the capacity of 2.06 kg/h peak operation and daily 11.26 kg according to Ref. [36], according to H_2 load profiles presented in Fig. 4. The designed hybrid system is also responsible for supplying the thermal load of a small residential building for a peak load of 2.09 kW and an average 11.26 kW h/d. The thermal load is going to be supplied by the boiler and 60 % of recuperated heat from the fuel-cell operated own-sized generator. The thermal load serves a typical residential building with 5500 square feet and 1 floor (total heated area of 5500 ft^2 (≈511 m^2)). The occupancy schedule is for weekdays: unoccupied from 8:00 to 17:00 (work hours), occupied in the evenings and at night, and mostly occupied during weekends. For the indoor design temperature, the heating setpoint is 21 °C. The more elaborate design characteristics based on typical cold-climate housing standards are mentioned in Table 1.

Table 1
Typical residential building specifications for a heating load.

Building Envelope (based on cold-climate construction):	
Walls	Insulated wood-frame walls, U-value ≈ 0.28 W/m^2·K
Roof	Well-insulated pitched roof, U-value ≈ 0.18 W/m^2·K
Floor/Slab	Insulated slab-on-grade, U-value ≈ 0.35 W/m^2·K
Windows	Double-glazed, U-value ≈ 1.2 W/m^2·K
Internal Gains:	
Lighting	5 W/m^2
Appliance & Equipment	8 W/m^2
People	100 W/person (sensible + latent)
Outdoor Design Temperatures (based on the Arctic port climate zone):	
Winter	T = −20 °C
Summer	T = +18 °C

The average wind speed profile for the Tromso and Lofoten area in northern Norway is shown in Fig. 5 a/b according to the NASA prediction of worldwide energy resource (POWER) database (Windnavigator is chosen for improved wind modelling). The improvement in wind energy

a)

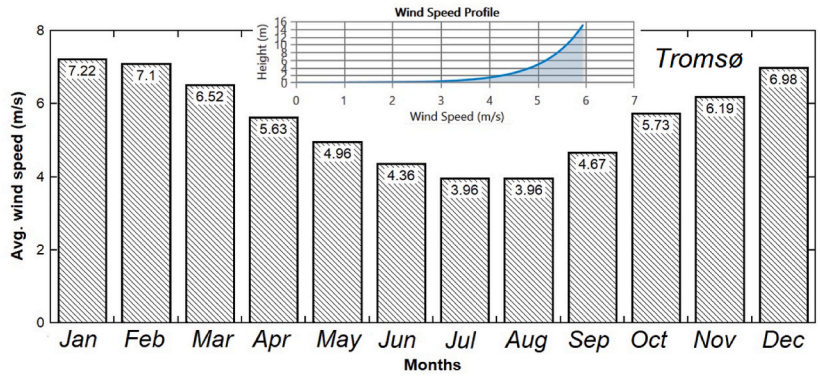

b)

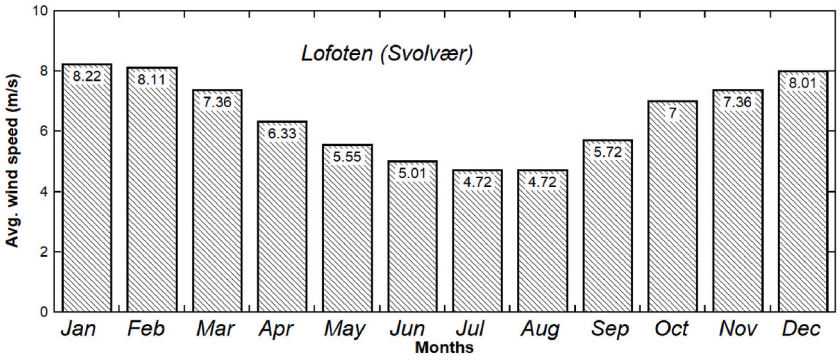

c)

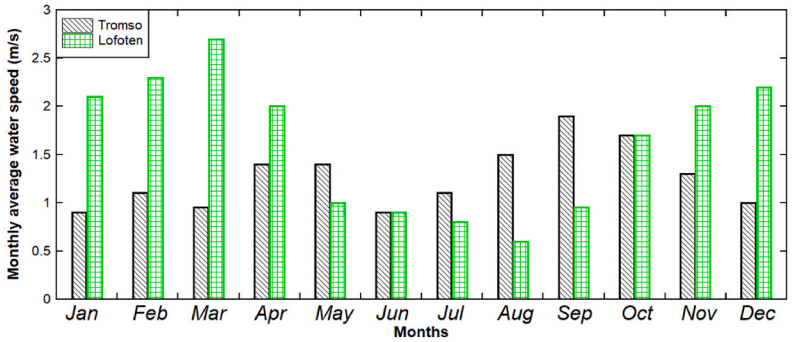

Fig. 5. Average monthly wind and wave speed data for Tromso and Lofoten.

resource production is available on this platform in the form of time series data. The scaled annual average in Tromso is 5.61 m/s, whereas at the Lofoten site, this value reaches 6.51 m/s. Lofoten archipelago shorelines are exposed to stronger onshore and offshore wind power compared to Tromso (the most intensive wind span is during the cold seasons). The wave hydrokinetic potential provides a sustainable renewable energy source that is especially fit to be harvested by HKTs deployed along the extensive Norwegian shores. Wave data, including significant wave height and direction, wave speed, wave period, and wave energy, are available online [37,38] and can be averaged for our two sites of interest to monitor during the months of the year. These data are collected and plotted in Fig. 5c, where the monthly average water/wave speed for Tromso and Lofoten is compared. There is a direct correlation between the wind and wave speed trend (Fig. 5: wind and wave speed plots with the highest frequency during the colder seasons). This highlights the significance of energy storage during the summer, when the intermittent renewable energy sources fail to meet the electric loads with the highest CS traffic. The scaled annual average of wave speed for Tromso and Lofoten is 1.51 and 1.6 m/s, respectively, which shows Lofoten is slightly better in wave energy utilization. Although the

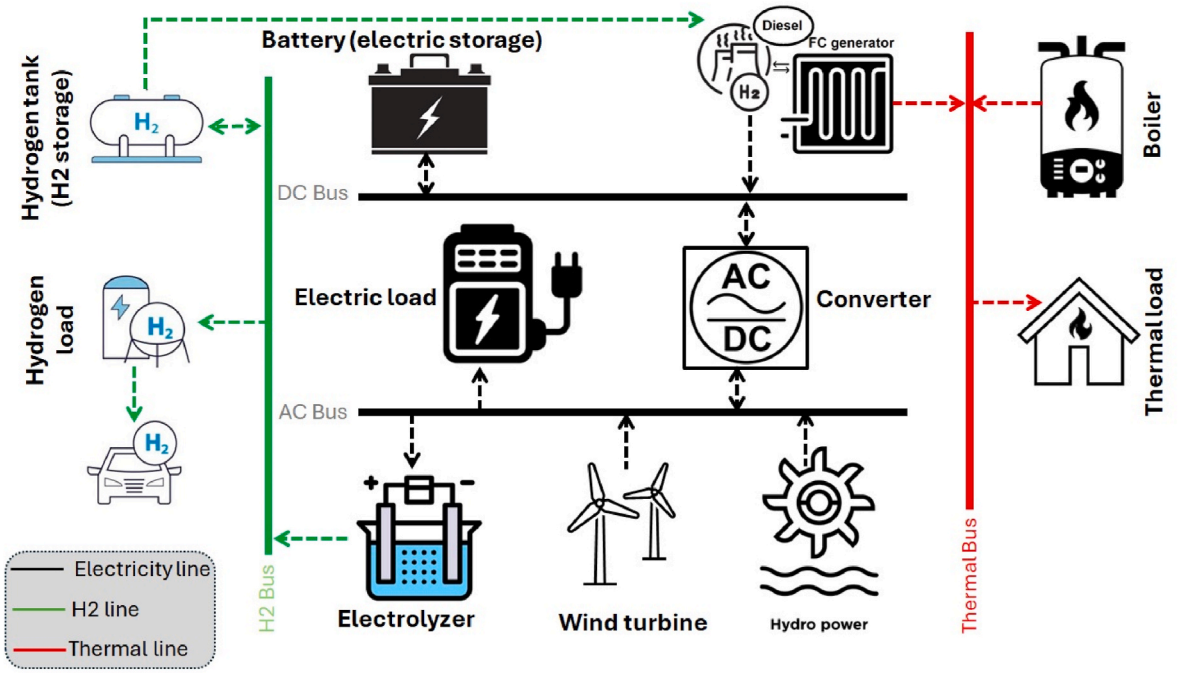

Fig. 6. Off-grid hybrid system architecture with a novel H_2 loop configuration using wave/wind potential serving the cold-ironing, H_2_FCEV, and thermal load.

Lofoten region displays a higher average wave speed, Tromsø's wave energy profile is more stable and shows less variability, especially during winter. This consistency promotes the reliability of power supply, resulting in improved capacity factor and dispatch control, while Lofoten requires more buffering or hybridization in design.

4.2. Hybrid energy system architecture

The architecture of a designed hybrid renewable energy system (HRES) is depicted in Fig. 6, which is composed of a Hydrogen tank, Hydrogen load, wind turbine, hydrokinetic turbine, fuel cell generator, electrolyzer, battery storage bank, electric load, converter, boiler, and thermal load. The system is designed to meet the electric load as a primary load, with hydrogen and thermal load as auxiliary loads. In addition, there is a load following (LF) controller, which operates based on a dispatching strategy to produce enough power by the generator for the primary load in the first place, and then the secondary loads are responded to by renewable power sources. The emphasis is put on the energy storage via battery and hydrogen generation and storage in a hydrogen tank. As shown, a good recirculation of electricity, hydrogen, and heat is established. Surplus electric energy is used in the electrolyzer to produce hydrogen. Hydrogen is either served for a hydrogen load or used in the hydrogen tank. Part of the hydrogen in the HTank is reused in an FC Gen operated with the stored H_2 and diesel fuels. On the other hand, FC Gen uses the same fuel to produce electricity, and a share of surplus electricity is used to be stored in a battery bank. A novel configuration of a hybrid energy system is a setup that minimizes the energy loss. Besides this, an optimization method is designed to minimize the excess electricity and maximize H_2 production and economic feasibility. Cruise ship load is considered baseload for cold ironing, whereas residential demands and hydrogen are regarded as auxiliary loads. The hydrogen fueling station is operated dynamically to absorb surplus generation during low-demand periods.

4.3. System component models

To estimate the overall performance of the hybrid system, each component has to be mathematically accounted for in the governing equations. System modeling is essential for energy and economic assessments.

4.3.1. Electrolyzer

A generic electrolyzer is employed, featuring a primary capacity of 100 kW, a 15-year lifetime, and an 85 % efficiency. A proton exchange membrane (PEM) type of electrolyzer is considered, which uses the excess renewable energy of wind-hydro coupled sources to convert water to Hydrogen through an electrochemical process. To represent this conversion, the electrolyzer efficiency is defined as [39,40]:

$$\eta_E = \frac{HHV_{H_2} \times \dot{m}_{H_2}}{U_{cell} \times I \times t} \tag{1}$$

Where $\dot{m}_{H2}$ represents the hydrogen production rate (in kg/h), U_{cell} is the cell voltage (typically ranges between 1.6 and 2.2 V), I is the current density (in Amperes (A)), and t represents the simulation time step in hours. Note that the denominator in Eq. (1) accounts for the power input. The high heating value (HHV) of H_2 or the energy content of this substance (when the H_2 in the product is in a gaseous state) is 39.4 kW h/kg.

4.3.2. Battery

The idealized battery model is used for excess electric energy storage, where it is possible to set the energy and power size independently. The selected battery package is a generic lithium-ion with 100 kW h of energy storage, a nominal voltage of 600 V, and a round-trip efficiency of 90 %. For the battery modeling, the maximum charging and discharging power is computed. These computations are decided according to the battery state of charge (SoC) as well as recent charge and discharge histories. The controller in each time step decides when to absorb the energy from surplus renewable power sources and when to discharge the stored energy to the loads. The battery's charging and discharging SoC (in %) at each time step can be expressed as [41]:

$$\begin{aligned} SoC_{batt}(t)|_{@charging} &= SoC_{batt}(t-1)(1-\alpha) + [\eta_c(P_{tot}(t) - P_{conv}(t))] \\ SoC_{batt}(t)|_{@discharging} &= SoC_{batt}(t-1)(1-\alpha) - [\eta_d(P_{conv}(t) - P_{tot}(t))] \end{aligned} \tag{2}$$

Where P_{tot} denotes the total hybrid system power generation in kW (here, a combination of WT, HKT, and $FC\ Gen$). The converted power

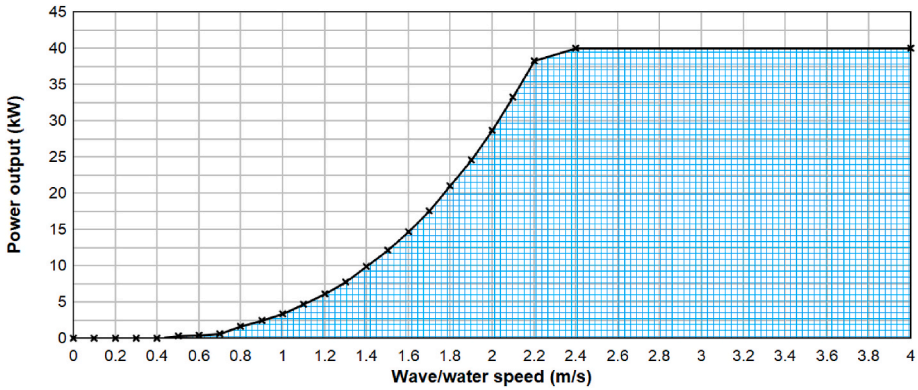

Fig. 7. Hydrokinetic turbine (HKT) power curve (power output vs. water speed).

between the AC/DC bus, considering the converter efficiency and the load demand, is shown with P_{conv}. In addition, α, η_c, and η_d are the battery's self-discharging rate and charging and discharging efficiency.

4.3.3. Hydrokinetic turbine

The nominal hydrokinetic turbine is integrated into the hybrid power system. This generic hydropower system is HK40 (40 kW capacity), which is a generic hydrokinetic turbine that captures tidal or wave energy with a negligible head. The generated power with the designed turbine for hydrokinetic energy corresponds with the turbine power curve displayed in Fig. 7, which shows how much power is produced with water/wave speed (kinetics). The hydrokinetic conversion systems extract the kinetic potential of waves/currents to calculate the maximum power [42]:

$$P_{HK,\max} = \frac{1}{2} C_{PE} \rho A V^3 \tag{3}$$

Where ρ is the water density, A is the turbine swept area (usually circular area), and V is the water velocity. C_{PE} is the overall power coefficient or turbine efficiency ($C_{PE} \leq 0.59$ based on the Betz limit stating the maximum threshold of fluid Stream Energy capture by an ideal turbine [43]).

4.3.4. Wind turbine

The same power curve is applicable for wind turbines, where an electric generator is coupled to convert the mechanical energy to AC electricity. The power curve approximation follows the equation below for wind speed [44]:

$$P_{WT}(t) = \begin{cases} 0 & u(t) < u_{ci} \\ a_1 u^3(t) + b_1 u^2(t) + c_1 u(t) + d_1 & u_{ci} \leq u(t) < u_1 \\ a_2 u^3(t) + b_2 u^2(t) + c_2 u(t) + d_2 & u_1 \leq u(t) < u_2 \\ a_3 u^3(t) + b_3 u^2(t) + c_3 u(t) + d_3 & u_2 \leq u(t) < u_{co} \\ 0 & u(t) > u_{co} \end{cases} \tag{4}$$

The wind turbine power (P_{WT}) is a time-dependent function of polynomial expressions based on wind speed at hub height $u(t)$ under different wind speed limits (i.e., u_{ci} and u_{co} as cut-in and cut-out wind speeds along with two consecutive speeds of u_1 and u_2 to increase the approximation precision).

4.3.5. Fuel-cell generator

The generic own-sized fuel-cell generator is used in the hybrid system that is operated with the stored hydrogen in the HTank. The heat recovery ratio from a combined heat and power (CHP) system is regarded as 60 %. The hydrogen consumed from the HTank by FC Gen is estimated as:

$$\dot{m}_{H_2} = \frac{N_{cell} \times U_{FC} \times I_{FC}}{\eta_{FC} \times LHV_{H_2}} \tag{5}$$

The FC Gen outpower (P_{FCG}), i.e., the numerator of Eq. (5), is modeled with the number of cells in a stack (N_{cell}), a single fuel cell voltage (U_{FC}) in V, and the current across the fuel cell stack (I_{FC} in A) parameters. In addition, η_{FC} is the fuel-cell efficiency, and LHV_{H2} represents the hydrogen fuel's lower heating value in MJ/kg. Only 60 % of the total heat generated in FC CHP, as formulated below, is recuperated to be used in a boiler.

$$Q_{FCG} = (\dot{m}_{H_2} \times LHV_{H_2}) - P_{FCG} \tag{6}$$

Where m_{H2} is the hydrogen mass flow from the HTank and LHV is the hydrogen low heating value equal to 120 MJ/kg.

4.4. Cost and economic modelling

The total system cost (net present cost: NPC) is the sum of each component cost. Each component cost is composed of three main constituents, namely capital cost (or capital expenses: CAPEX), replacement cost (when the project lifetime exceeds the component service life), and operation and maintenance cost (OPEX). These costs must be updated to changes in future years' discount ratio, and that is when the annualized cost (C_{ann}) parameter is involved in the economic analysis. The component and total system NPC are as follows (the total NPC is the sum of the NPC of all components involved in the designed hybrid system) [45]:

$$C_{NPC,\text{component}} = C_{capital} + C_{replacement} + C_{\text{O\&M}} \tag{7}$$

$$NPC_{tot} = C_{NPC,electrolyzer} + C_{NPC,\text{Htank}} + C_{NPC,WT} + C_{NPC,\text{HKT}} + C_{NPC,FCGen} + C_{NPC,conv} + C_{NPC,Batt} + C_{NPC,Boiler} \tag{8}$$

The annualized total NPC cost will then be

$$C_{ann} = CRF \times NPC_{tot} \tag{9}$$

Where CRF is the capital recovery factor, which is the function of the project lifetime in years (n) and discount ratio (IR in %).

$$CRF = \frac{IR(1+IR)^n}{(1+IR)^n - 1} \tag{10}$$

The levelized cost of energy ($LCOE$) and levelized cost of hydrogen ($LCOH$), which are used as the sub-objective functions of second-step optimization, are defined as:

$$LCOE = \frac{C_{ann}}{\sum_{t=1}^{8760} P_L(t)} \tag{11}$$

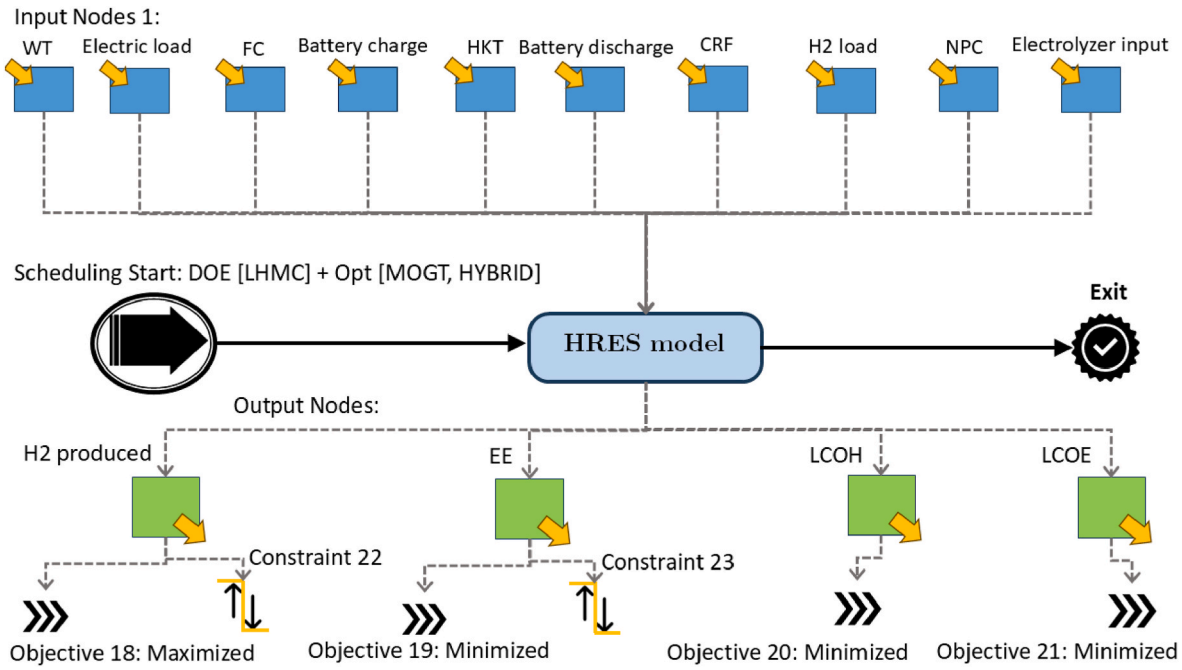

Fig. 8. DOE and optimization algorithms diagram.

$$LCOH = \frac{C_{ann}}{\sum_{t=1}^{8760} H_{2,L}(t)} \tag{12}$$

Here, $P_L(t)$ is the load power sum over a year based on hours of the system operation, and $H_{2,L}(t)$ is the hourly sum of hydrogen load/demand. Accordingly, the excess electricity (*EE*) is calculated as:

$$EE = \sum_{t=1}^{8760} \left[P_{WT}(t) + P_{HKT}(t) + (\eta_{conv} \times P_{FCG}(t)) - (\eta_{conv} \times P_{batt,ch\ arg\ e}(t)) + (\eta_{conv} \times P_{batt,disch\ arg\ e}(t)) - P_{electrolyzer}(t)\right] \tag{13}$$

The converter efficiency is represented by $\eta_{conv} = 0.95$, and battery charging and discharging power connected to the hybrid off-grid system are shown by $P_{batt,\ charge}$, and $P_{batt,\ discharge}$ in kW.

4.5. Computational methods

4.5.1. Design of experiments (DOE) sampling

Engineering optimization consists of an experiment that is a set of variations in the input based on a specific rule to change the output in a desired direction. This is why the preliminary sampling of the input variables in the design domain is an overarching concept in the optimization methodology. The selection of the initial scattered input data (design space) is called the design of experiment (DOE). DOE features a smart design space exploration while decreasing the time and effort necessary for conducting the experiments. The combination of DOE with optimization is practiced in the current HRES configuration since DOE outlines the behavior of the objective function by identifying which factors are the most significant. The selection of a DOE relies chiefly on the type of objectives and the number of variables involved.

The Latin Hypercube-Monte Carlo (LHMC) from the robustness and reliability cluster is chosen to operate DOE samplings. For each variable, the points are randomly distributed. Latin Hypercube is useful when a random sample is needed. It guarantees to be relatively uniformly distributed over each dimension. The LHMC serves to evaluate the effects of the random variability of certain factors on the responses. They are used for generating statistical distributions of multivariate distributions and are thus particularly suitable for robust design optimization [46]. In the adopted DOE scheme, 25 designs are taken with the Latin Hypercube Sampling (LHS) scheme. The statistical distribution is split into *n* intervals with the same probability, and a random value is selected in each interval according to the density function. In this way, points are relatively uniformly distributed over the density function range. On the other hand, the Monte Carlo sampling chooses *n* values independently according to the global uniform density function. Furthermore, compared to Monte Carlo, LHS maps better the *marginal probability distributions* (i.e., the statistical distribution of each single variable), especially in the case of a small number of generated designs. LHS is, therefore, more efficient in reproducing a distribution with fewer samples than Monte Carlo.

DOE is used for RSM training and optimization in this study. For the RSM training purpose, adequate datasets will be generated to enable the creation of reliable response surfaces. The dataset's uniform distribution in the design space must be as high as possible, and the more samples, the better the RSM reliability. In the optimization context, DOE provides a good starting point with a suitable input data population. For each optimization algorithm, a different DOE with a different size can be applied.

4.5.2. Multi-objective game theory (MOGT) optimization

The first optimization algorithm is multi-objective game theory (MOGT) and is chosen from the heuristic optimizer class. The MOGT is based on game theory, and its first application appeared in economics. This optimization method is particularly recommended for highly constrained and non-linear problems. The algorithm is a competition between players who are responsible for optimizing a task to achieve an objective they are tasked with. The game results are determined based on the Nash equilibrium [47], which states that no strategy change is acceptable if other players remain unchanged. MOGT launches the process with the preliminary designs of the DoE configuration, while other entries are skipped. Every internal simplex demands $n+1$ initial designs, where n represents the number of input variables linked to a specific player. The MOGT operations end once the maximum number of player steps is reached or the desired accuracy is established. This algorithm features automatic decomposition of the variables' space among the players. It also allows concurrent evaluation of

configurations proposed by each player. The number of objectives should not be greater than the number of variables. The algorithm is configured by self-initializing, and the number of evaluations is set to 200 for this research. This algorithm manages constraints by employing the constraint domination technique.

4.5.3. Hybrid multi-strategy optimization

The second optimizer is HYBRID from multi-strategy algorithms classification that combines the global exploration features of Genetic Algorithms with the precise local exploitation secured by sequential quadratic programming (SQP) implementations. The SQP solver is a filter that works on a scalarized version of the original problem obtained through an improved epsilon-constrained technique. The internal archive (used mainly for RSM training) is initialized using the designs already listed in the design space table. Like the previous optimizer, the algorithm is configured automatically through self-initializing with 200 evaluations.

The DOE incorporation with optimization concept procedure applied on the proposed hybrid off-grid system with inputs/objectives/constraints is illustrated in the block chart of Fig. 8.

Although average wind and wave data are used for optimization on a monthly basis, the application of Latin Hypercube–Monte Carlo (LHMC) sampling causes statistical variability across environmental and design parameters. The analysis allows the model to capture a wide range of input uncertainties, particularly in resource-dependent variables.

4.6. Virtual optimization: RSM and AI metamodels

Response Surface Models (RSMs) or metamodels represent/approximate statistically the input and output behavior of the system. In this way, a limited number of designs are run to form a mathematical function so that the behavior of responses can be predicted. According to the behavior of input values, the RSM algorithm estimates the value of the unknown output function based on an assumption. The optimization afterward will be carried out with this function instead of the real solver to find the combination of input values that leads to an optimal response (The virtual optimization responses). The RSM-based optimization explores the design space with a surrogate model instead of the real objective function. The virtual responses (the response surface) are the approximations made by the surrogate model. An RSM-based optimization yields quicker results because the response surface is an analytical function. The RSM algorithms are classified into interpolating and approximating categories. In this study, multi-layer perceptron (MLP) and neural networks (NN), which approximate RSMs, are utilized. This does not pass precisely through the training data but minimizes the extrapolation error on the training points.

The NN relies on statistical learning data processing for the estimation of the functions. Neural Networks are comprised of multiple adaptive weights and biases (numerical parameters tuned by the learning algorithm). Back-propagation during the learning procedure means the comparison of the RSM-estimated output values with the real output values of the training set to calculate the prediction error. In each numerical iteration, the weights are adjusted suitably to minimize the prediction error, i.e., mean squared error. This internal optimization is performed using the Levenberg-Marquardt algorithm [48] for a fixed number of iterations. All variables, both input and output, are normalized internally, which is fundamental for the RSM training. Neural Network weight initialization is performed with the Nguyen-Widrow technique [49], which greatly reduces the training time. NN is employed as a metamodel optimization as a virtual optimizer compared to the MOGT real optimizer, for an objective function consisting of EE, H_2 production, LCOE, and LCOH (simulating LHMC-MOGT design space).

On the other hand, for the LHMC-HYBRID real optimizer, the MLP virtual solver is adopted based on the H2O.ai platform (deep learning). This network is trained with stochastic gradient descent using backpropagation. The network encompasses many hidden layers of neurons with a tanh activation function. Advanced features such as adaptive learning rate, rate annealing, momentum training, dropout, L1 or L2 regularization, checkpointing, and grid search ensure high predictive accuracy. MLP uses 5-fold cross-validation on training data (metrics computed for combined holdout predictions), and the status of neuron layers is based on regression and Gaussian distribution.

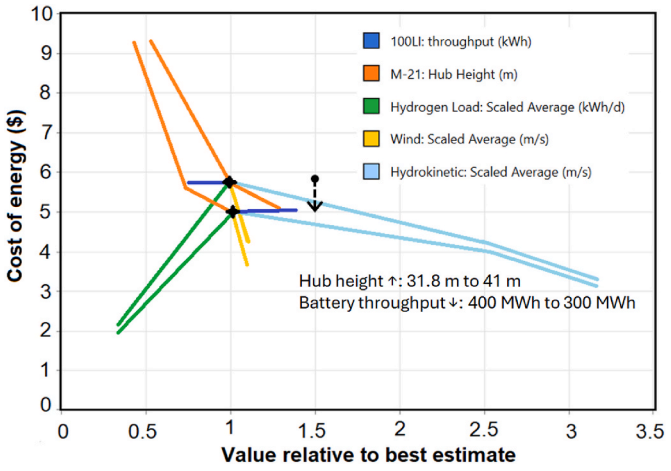

Fig. 9. Spider plot for COE based on various sensitivity variables.

For training the RSM configurations, the following steps are taken: first, the selected feasible designs are selected to ensure the best points are used for the training. Then, error designs are excluded, and repeated designs are removed. In the second step, the validation table is defined to perform the RSM validation (20 % of data, i.e., 40 of 200, are used randomly for this purpose). In the third step, the input and output variables are selected, and finally, RSM functions are created and configured as metamodel optimizers.

5. Results and discussions

5.1. Sensitivity analysis and optimal system configuration (based on internal optimization)

The spider plot is a pragmatic method of sensitivity analysis of design inputs to understand which parameters have a significant impact on desired dependent variables. The spider graph in Fig. 9 displays the design parameters' relative change to best estimate that these parameters are put in three categories of resources (wind and hydrokinetic), load (hydrogen load of the hybrid system), and components engineering (battery throughput and wind turbine's hub height). At any given input variable, the spider graph can be generated to show the range of COE concerning the extended legs of design inputs. The hydrogen load decrease influences the COE reduction drastically, and this parameter is the most sensitive factor, while the battery throughput is not very dominant since its variation does not influence the COE. An increase of 22.4 % of WT hub height brings down the optimal center for COE alone by about $0.8. The WT hub height ranks second in terms of the impact on the cost of energy. Scaled hydrokinetic wave speed variation is considered in a wider range (3.3:1), and this causes only a 29.3 % COE reduction. However, the hub height variation span is in a short range, and the slight increase from the baseline (31.8 m) decreases the COE, while a hub height decrease from the baseline leads to a 37.6 % increase in COE. It can be assumed that the resources variation comes after the load regulation and component sizing in terms of COE and economic significance. On the other hand, the scaled wind line has the steepest slope and has the potential to influence the COE severely, but its range is limited since the wind speed average cannot be changed extensively.

The optimal system type zoning or partitioning based on different

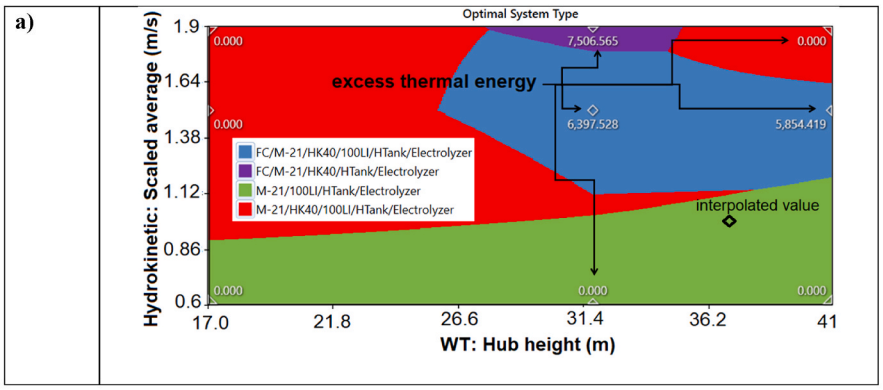

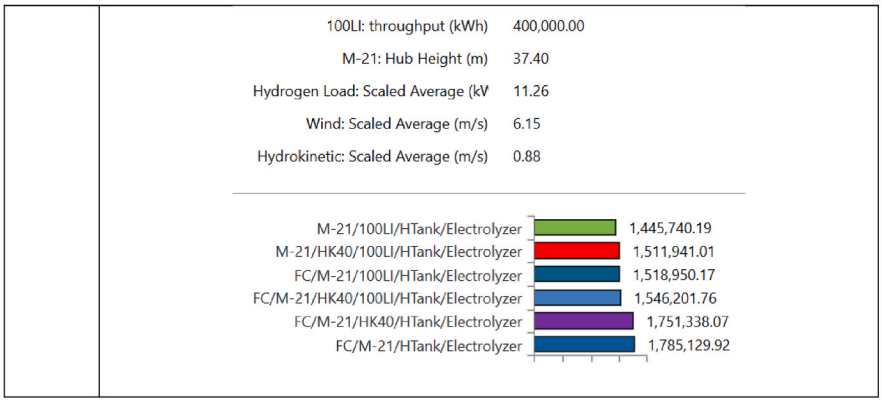

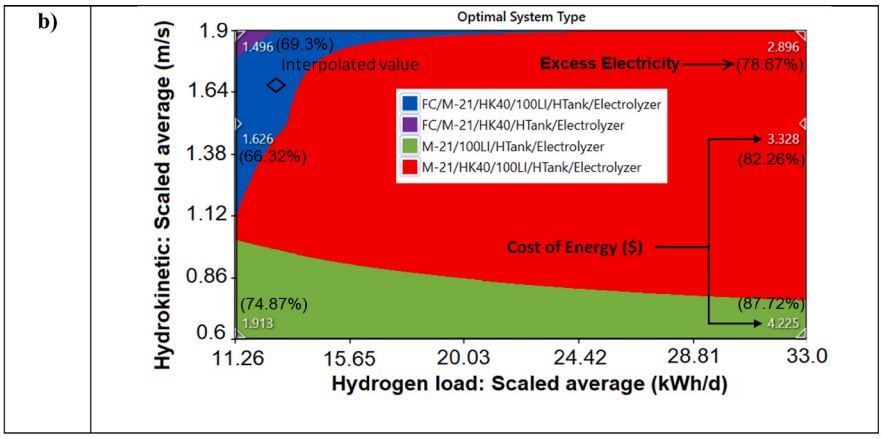

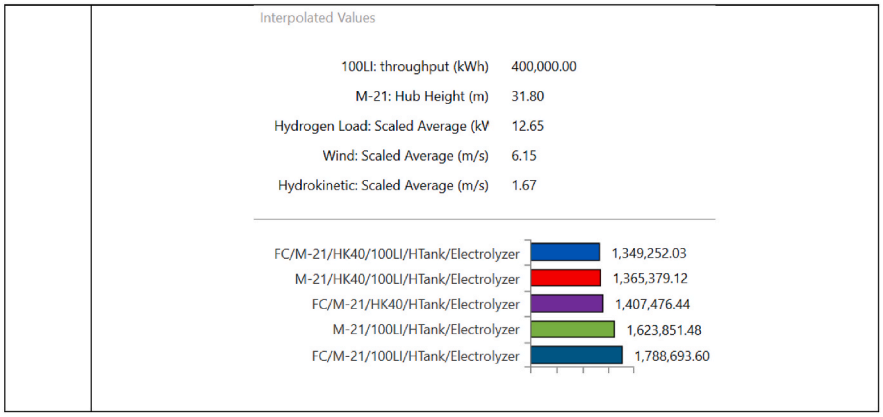

Fig. 10. Optimal system type: a) partition based on the scaled hydrokinetic speed vs. Hub height, and b) partitioning based on the scaled hydrokinetic speed vs. Hydrogen load.

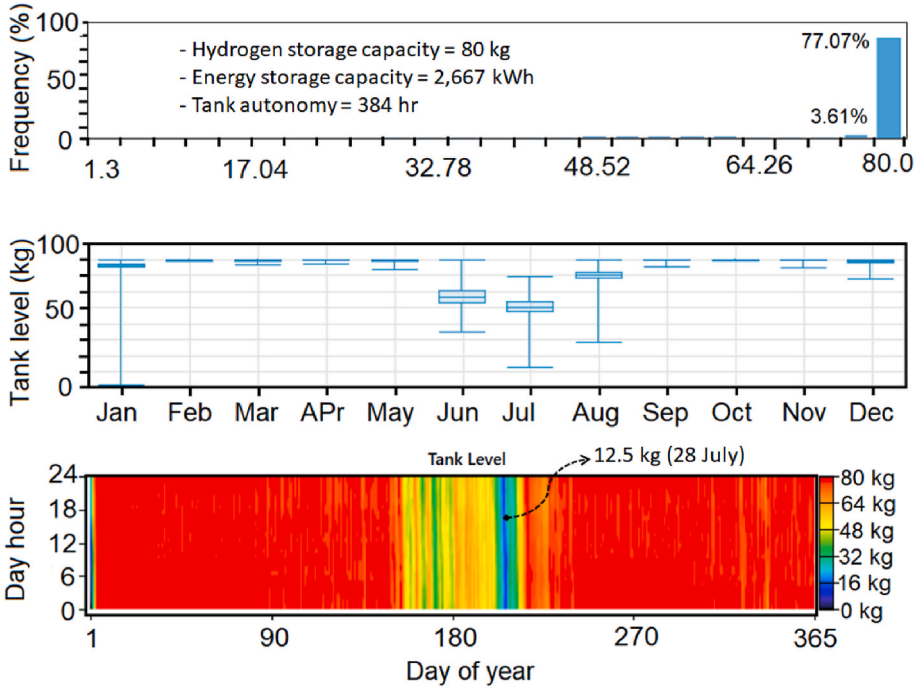

Fig. 11. Hydrogen tank profile for the best optimal architecture.

input parameters is shown in Fig. 10, where the output values are superimposed. Different zones representing different hybrid system configurations (architectures) are colored and separated according to different scaled HK water speed and WT hub height in the first case, i.e., Fig. 10a. The graph implies that when the HK source of water speed is less than the scaled average of 0.88 m/s and under any WT hub height (green area), the FC Gen and HKT components are not required, and therefore they are not considered economically viable. It can be noted that in a blue and pink area where FC is involved, there is excess thermal energy that is transferred to the boiler and the thermal load. In the blue region (with FC and battery), the excess thermal energy is 14.7 % less than the pink region's excess thermal energy (with FC and without battery) since the battery can capture a share of the excess energy. Increasing the hub height of WT in the blue region can further reduce the excess thermal by 8.4 % (6397.5 → 5854.4 kW h/y) since the system receives most of the energy from the renewable wind, and the requirement for FC operation is lowered. In addition, the FC Gen operation with H_2 generates high heating value (LHV = 120 MJ/kg), and this surplus energy can be potentially used by a thermal storage unit. The thermal load controller and thermal storage system are not used for the under-investigation hybrid system since they incur costs and reduce the financial feasibility of the plant. The interpolated value with specified input design variables is identified in the system plot. The best configuration (in terms of NPC) with the components array shown with the green code (WT/Battery/Htank/Electrolyzer) equals to $1.44M, while the worst-case scenario is arrayed with FC/WT/HTank/Electrolyzer having NPC = $1.78M. The results indicate that using FC Gen without a battery as storage is costly and environmentally unfriendly.

The second optimal system identification graph is plotted with HK source availability and hydrogen load in Fig. 10b, while excess electricity and COE values are superimposed on the graph. It is recommended that when the hydrogen load is very low and the hydrokinetic water speed is high enough, FC would be incorporated and utilized in the microgrid system (the blue and pink region in the upper left corner of the graph). As hydrokinetic speed increases, more economic system configurations are proposed (e.g., from COE of $4.225 to $2.896 at scaled H_2 load = 33.0 kW h/d). The observation on this figure confirms that there is a correlation between COE and EE, so any attempt to reduce

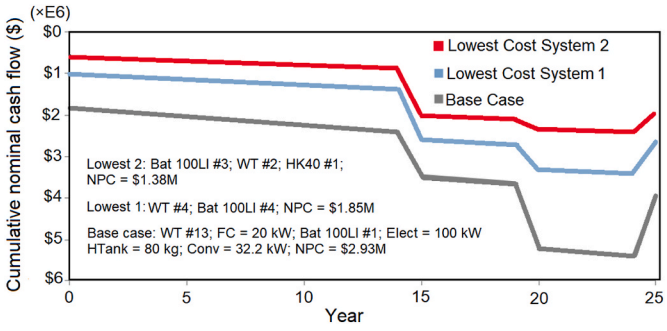

Fig. 12. The cumulative cash flow variation with the lifetime of the project for the base and low-cost scenarios.

the excess electricity leads to lower COE. Lower HK speed and higher H_2 load yield a significant electricity overproduction (over 87.7 %). This indicates that if the HK wave speed is not enough and yet there is a considerable demand for H_2, considerable investment is required in a series of WT and large battery capacity, and it will consequently ramp up the costs (higher COE). Regarding the interpolated value located in the blue region (design variables mentioned underneath the plot), the most economical configuration occurs when the combined system fits the FC and battery with NPC = $1.35M.

The HTank storage and capacity in the hybrid system are underlying characteristics that contribute to the reliability and resilience of renewable energy production and dispatch. The histogram, box plot, and heat map of hydrogen in an HTank with 80 kg capacity over a year duration are demonstrated in Fig. 11 for the optimal configuration (No FC with NPC = $1.1M). The hydrogen acts as an energy storage or energy carrier, and in this system arrangement, the HTank can store up to 2667 kW h of energy. The HTank, as illustrated, is filled to its full capacity most of the year. However, during the hot season, the hydrogen level drops (the lowest H_2 recorded at 12.5 kg on July 28) due to reduced wind and wave speeds, as well as high thermal and electrical loads. The histogram indicates (in 77 % of cases) that the HTank is full of 80 kg H_2 (in July, the HTank reaches its lowest mean storage of 50.0 kg).

Table 2
Best system configuration scenarios: first-step optimization results.

Ranking	WT (M-21) #	FC (kW)	Battery (100LI)	HK40 #	Converter (kW)	COE ($)	RenFrac (%)
	Config1: No FC (Min. NPC = $1.1M)						
1	1	–	2	1	31.6	1.4	93.7
2	2	50	–	1	20.8	1.5	93.9
3	2	20	1	1	20.8	1.53	93.8
4	3	–	3	–	34.1	1.78	93.7
5	5	20	1	–	30.1	2.0	93.9
6	6	50	–	–	30.0	2.18	93.9
	Config2: No Battery (Min. NPC = $1.18M)						
1	2	50	–	1	21.1	1.5	93.9
2	2	20	1	1	21.1	1.53	93.8
3	2	–	2	1	240.9	1.56	93.7
4	3	–	4	–	31.0	1.91	93.7
5	5	20	1	–	30.9	2.0	93.9
6	7	50	–	–	30.6	2.39	93.9

The lifetime of the hybrid energy system establishment is considered 25 years, and Fig. 12 shows how the hybrid system saves money over the project lifetime for the base case and optimized cases. The cumulative cash flow diagram is illustrated under the lowest tuning design inputs, and the optimal cost systems are searched for HK wave speeds of 0.6 m/s and 1.9 m/s. The base case specification is mentioned within the plot that requires many WTs. The lowest cash flow systems 1 and 2 have noticeably fewer WTs. For the low-cost system1, more batteries are included, but no HKT is used since the scaled water/wave speed is low, so more batteries are used. When the HK source water speed increased to 1.9 m/s in system2, fewer batteries and WTs are integrated into the system, and HKT is included, which can reduce the energy production cost and increase the profitability of the plant for hydrogen generation and energy storage ($1.55M less NPC). This echoes the significance of hydrokinetic energy potential in the Arctic region for hydrogen production and off-grid electricity by wave energy.

The results of hybrid renewable energy system optimization for the first stage are gathered in Table 2 for the two main prioritized configurations (first without FC and second without battery storage). The rest of the priorities in combination of components in the hybrid system are WT/FC/Battery/HKT, then WT/Battery. The WT is present in all possible scenarios, and the optimal configuration is a scenario in FC that does not involve the hybrid system because high-value H_2 as a fuel is used to meet the thermal load, which can be supplied by using cheaper diesel fuel or natural gas with higher emission considerations. The first step of optimization ranks different sub-permutations with the proposed sizing (number and capacity) of the system, as indicated in the table below. The collected data in the table reveals that excluding the battery and HK leads to relying heavily on FC Gen and WT, and this increases the overall costs of the system and energy cost.

5.2. DOE/external optimization, and RSM results

The second step of optimization is performed on the best architecture of the hybrid system, including all components. The multi-objective algorithms then attempt to minimize the energy efficiency (EE), levelized cost of energy, and hydrogen production while increasing hydrogen production. The sub-objectives are weighted, with the primary emphasis on EE minimization ($w_2 = 3$). Then, hydrogen production is weighed ($w_1 = 2$), and then LCOE and LCOH ($w_3 = w_4 = 1$) as stated in the objective-function below:

$$\begin{aligned} Obj\_fnc &= F(w_1 \times Obj1 + w_2 \times Obj2 + w_3 \times Obj3 + w_4 \times Obj4) \\ &= F\left(2 \times \left(H2\_production\right)^{*} - 3 \times EE^{*} - LCOE^{*} - LCOH^{*}\right) \end{aligned} \tag{14}$$

*Scaled parameter.

The two sets of different optimization algorithms are applied with the same data size, DOE, and input parameters so that the performance of the two optimization algorithms can be compared (MOGT and HYBRID with LHMC as DOE).

The sub-objective values are normalized, and the objective function values are mapped to the plot in Fig. 13 for each design ID populated during the optimization. The two algorithms with different natures are clearly in competition to increase the objective values with ID evolution. In total, 198 designs are generated, and while having a close competition until DesignID63, MOGT succeeds in outdistancing afterward. The better performance of the MOGT optimizer is displayed by the linear fitting line having the steeper slope. MOGT optimizer finds the best design point with a higher value (Y = 2.94) sooner (X = 162) than the HYBRID algorithm (X = 198, Y = 2.5). MOGT is in the class of heuristic optimizers, whereas HYBRID is classified under multi-strategy algorithms. The first 24 candidates are DOE designs arranged by the LHMC scheme.

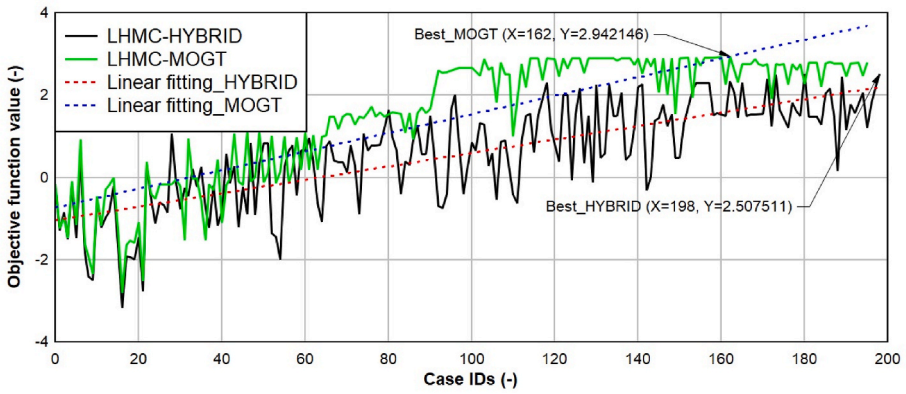

Fig. 13. MOGT vs. HYBRID optimization evolution with design case IDs, with initial DOE population and linear fittings.

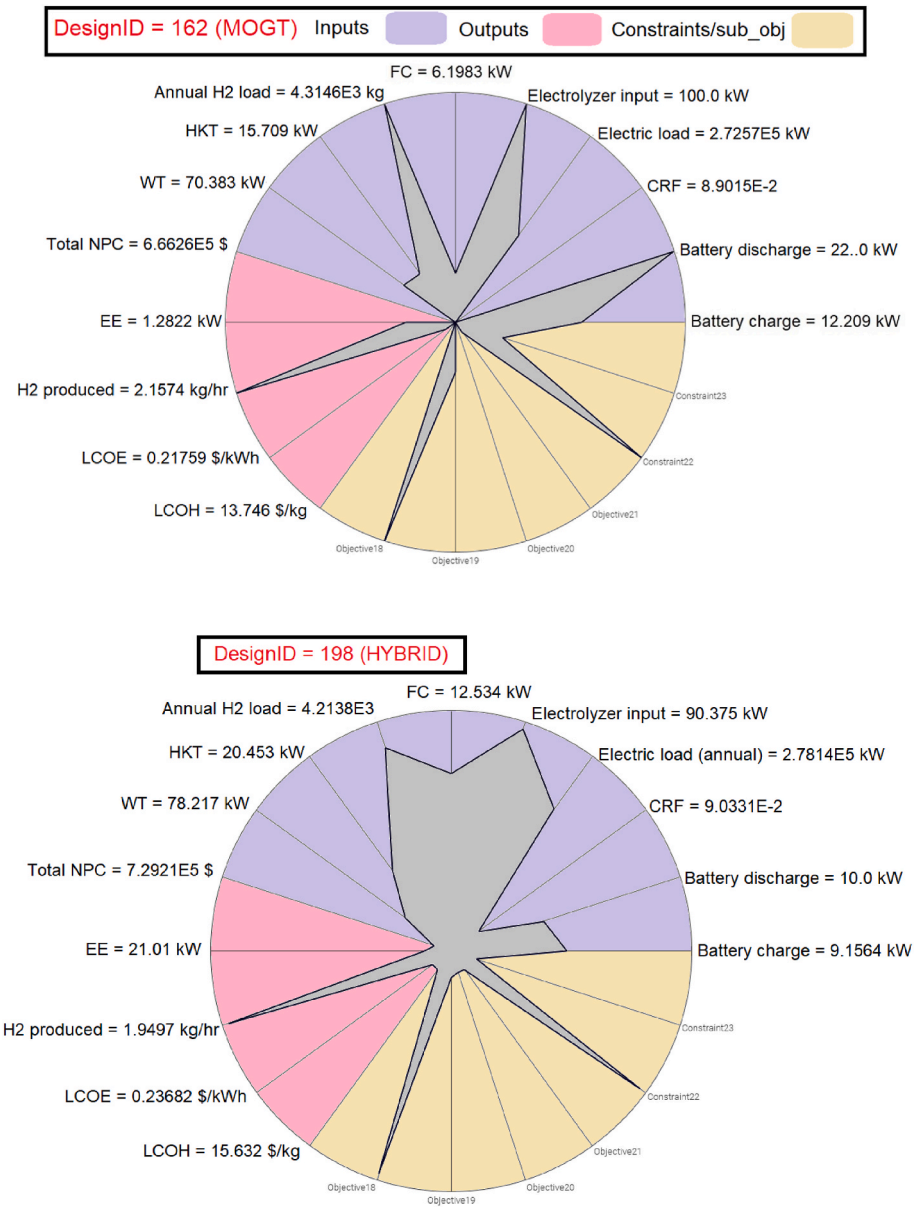

Fig. 14. Input-output values of the selected best designs of MOGT (ID162) and HYBRID (ID198).

This method can diversify the range and type of the proposed input data. The HYBRID algorithm integrates the steady-state GA with a controlled elitism procedure called sequential quadratic programming (SQP) instead of conventional operators of the GA algorithm. The adaptive filtering operation and simplex/gradient mechanism of the algorithm have proved to be slow compared to the heuristic optimizer. MOGT handles the conflicting agents of the multi-objective function and sets a good balance of exploring the design space and Pareto front identification.

The design variable values leading to optimal hybrid system configuration for both types of optimization algorithms are displayed in Fig. 14. The best design ID162 of MOGT results in a better outcome for EE, hydrogen production, LCOE, and LCOH compared to optimal design ID198 for HYBRID. The excess electricity is reduced to a minimal point of 1.28 kW, while the LCOH shows a very low level of 13.74 $/kg thanks to high hydrogen production and smart energy management between different hybrid system components. The power flow of HKT, WT, electrolyzer, and battery charge/discharge of the prominent design ID162 is significant to achieve the desired goal of the optimization. By adjusting the transient energy flow and energy management, it is possible to reach a better result than the first-stage HRES system first-step optimization (without FC Gen, NPC = $1.1M, LCOH = 20.4 $/kg). This shows that by adopting optimization, energy production by renewable and sustainable sources will be handled intelligently. Because the optimizer matches load demands and the energy stored in the HTank and battery. The second layer optimization by MOGT and HYBRID algorithms on the third-ranked architecture resulted in 32.6 % and 23.3 % LCOH reduction compared to the best design of the first-step optimization (No FC Gen). The key takeaway from the comparison of two optimal solutions is that MOGT is showcasing higher battery charge and discharge exchange capacity (thus lower EE) along with less FC output than HYBRID. This is indicative of less reliance on FC and more engagement of the storage system, thereby establishing a balanced renewable energy source. The hybrid best solution (compared to the

i)

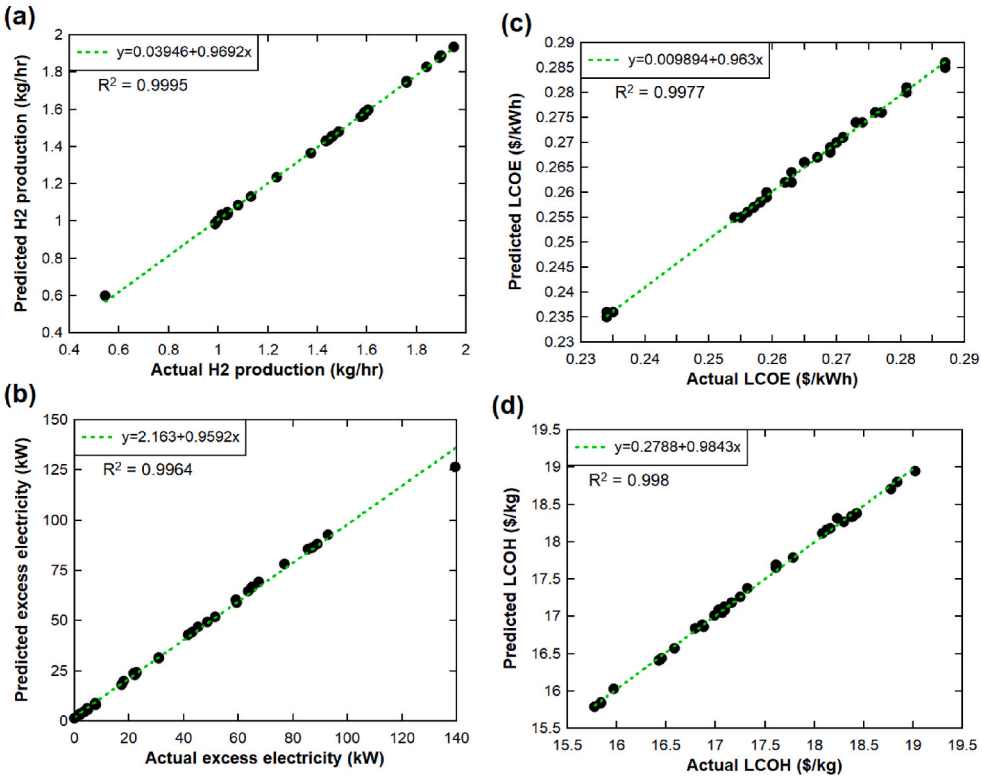

ii)

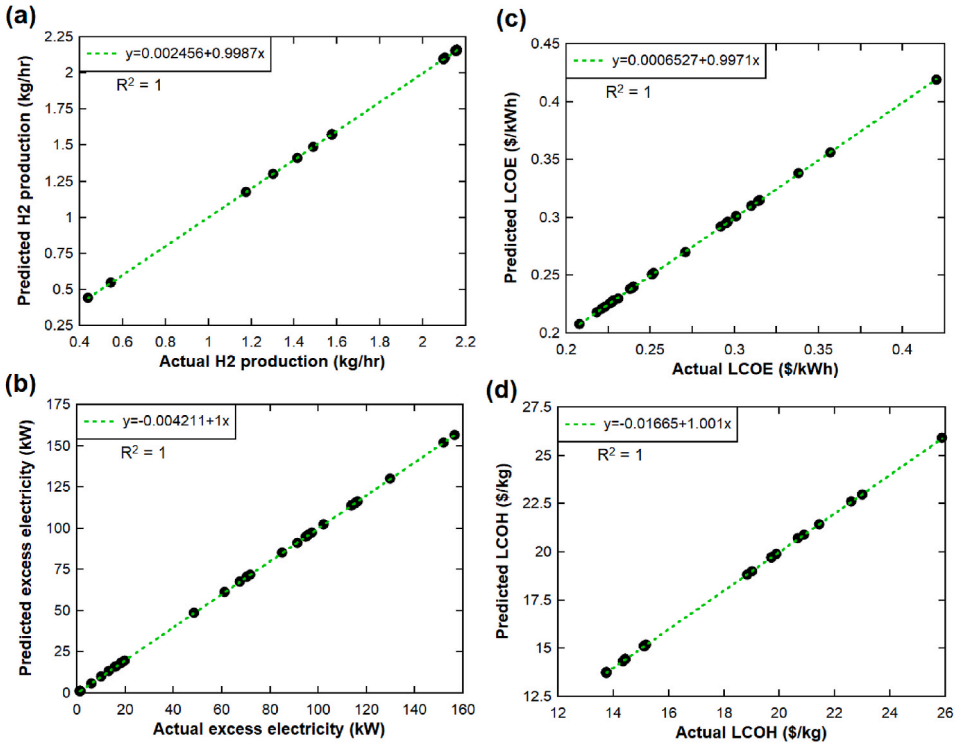

Fig. 15. Scatter plots of RSM with i) MLP and ii) NN for optimization outputs of a) hydrogen production rate, b) EE, c) LCOE, and d) LCOH.

Table 3
Error measures of RSM functions used for virtual optimization models in the hybrid renewable energy system.

	HYBRID (RSM function: MLP)		MOGT (RSM function: NN)	
validation error	MAE	MSE	MAE	MSE
Excess electricity	0.988	2.09683	1.599E-2	7.378E-7
H_2 production	1.001E-2	1.17534975E-4	4.451E-3	0.212E-7
LCOE	5.5156E-4	6.8711523E-7	1.378E-3	0
LCOH	3.4685E-2	0.0013190437	4.543E-3	3.0E-6

MOGT best solution) retains more HK and Wind power, entailing more economic investment (note NPC_{HYB} = \$729,215 < NPC_{MOGT} = \$666,265).

The modeled LCOH in the optimized framework ranges between \$13–\$20/kg, reflecting Arctic microgrid conditions with high CAPEX, seasonal intermittency, and logistical isolation. These values align with findings for remote, off-grid hydrogen systems.

The RSM is employed as a virtual optimizer using the input-output dataset generated during the actual optimization for training purposes. In other words, it is an approximation based on a predictive model developed by different AI methods built on an optimization population. Two predictive models were developed first for HYBRID cases using MLP (H2O.ai), and second, for the MOGT case points using NN. The meta-models are used to predict responses with untried input design configurations and perform optimization runs, trade-off studies, or further exploration of the design space.

The scatter plots for four sub-objectives are represented in Fig. 15i for MLP-HYBRRID and in Fig. 15ii for NN-MOGT. These validation scatter plots show the statistical reliability of the virtual designs, and in a general overview, NN outperforms MLP with $R^2 = 1$ for all sub-objectives of EE, H_2 production, LCOE, and LCOH. For the MLP training process, a 5-fold cross-validation on training data is implemented (metrics computed for combined holdout predictions). The predictive robustness for H_2 production is better with a higher R^2 =

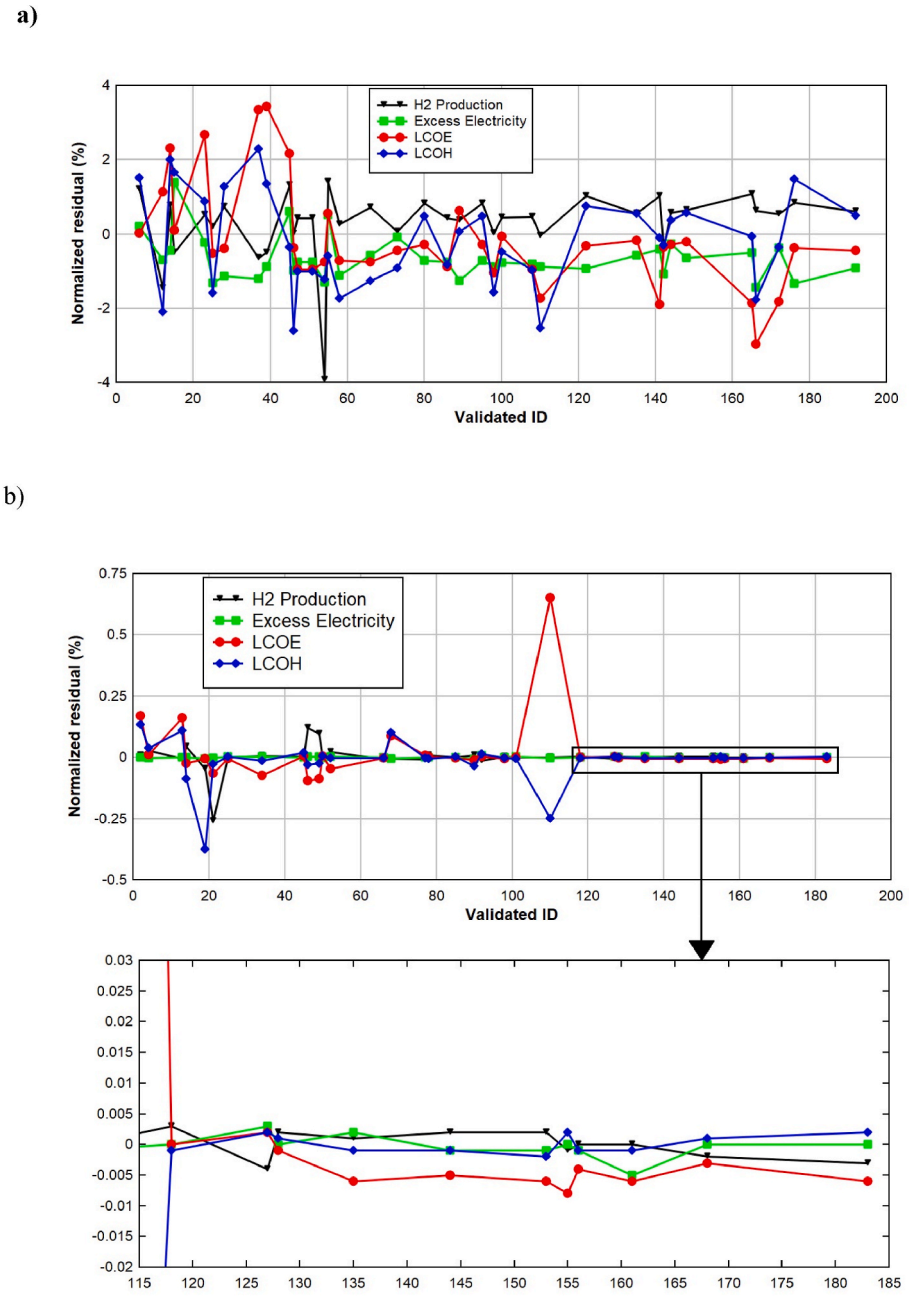

Fig. 16. Normalized residual variation with validation data for a) MLP training function and b) NN function.

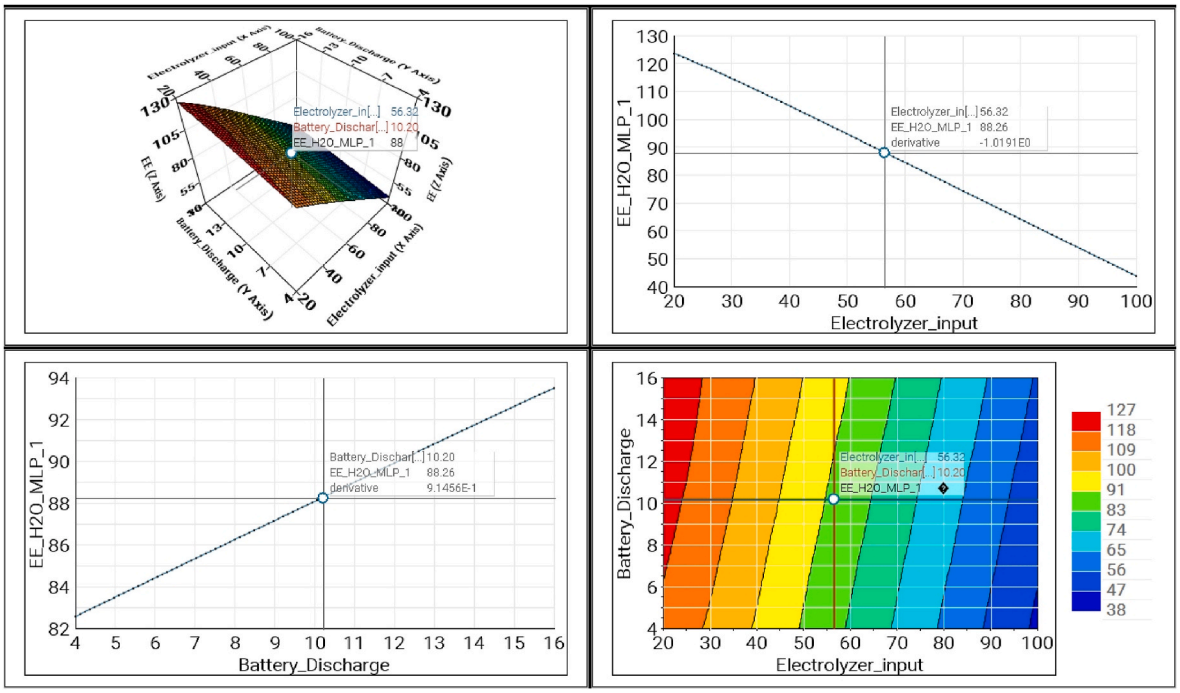

Fig. 17. 3D exploration plot for EE based on electrolyzer and battery power exchange.

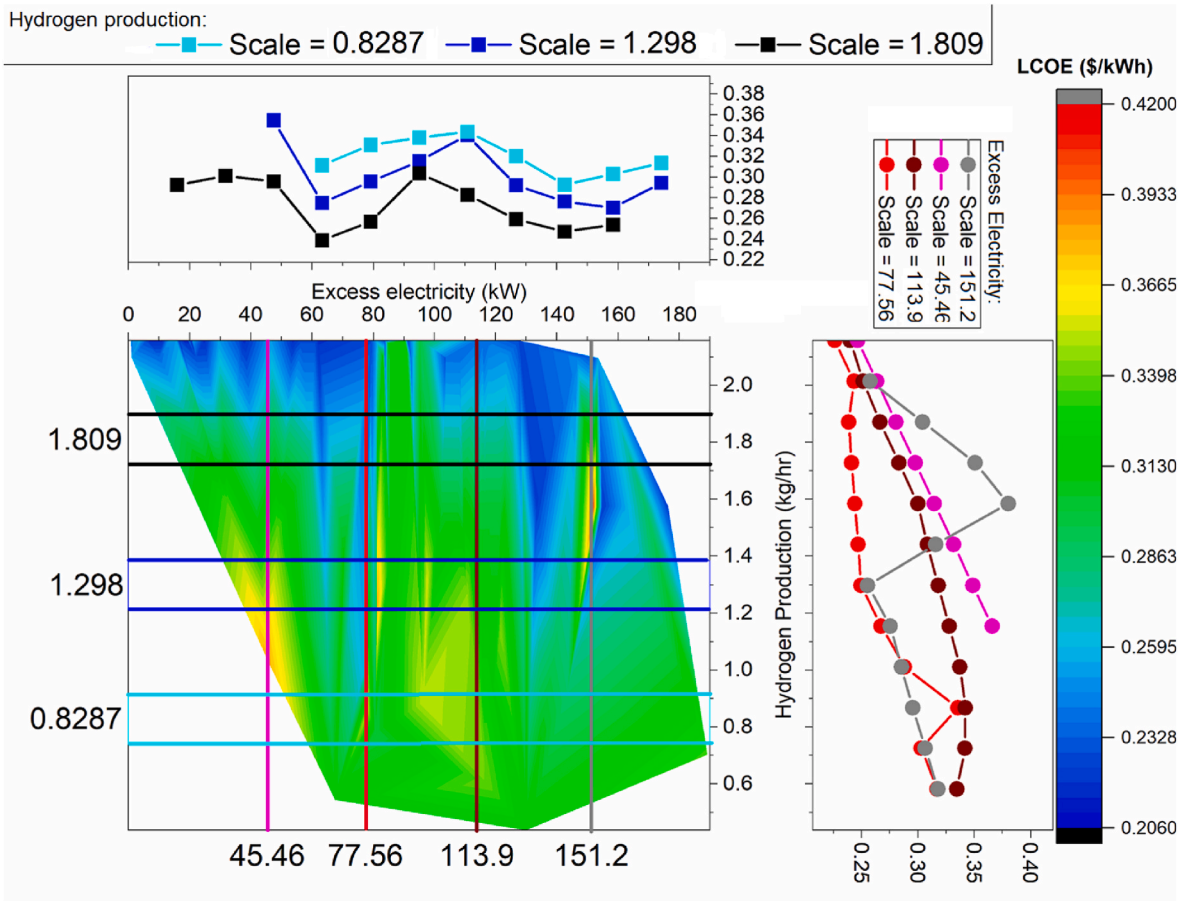

Fig. 18. Contour plot of the covariation of the RSM model objectives.

0.9995, and it is evident that for all objective outputs, the model can map the data on the unity line, demonstrating that the H2O model can produce the results with a high degree of accuracy. A total of 40 data points from 200 data sets are utilized for the validation of the RSM performance (500 neurons are used in the hidden layer). For the NN model, the number of neurons in the hidden layer is 8, and the degree of freedom is 97 (free network parameters computed by the algorithm).

The error metrics of mean absolute error (MAE) and mean square error (MSE) for the two RSM approximator functions are listed in Table 3. The generated output error by the NN is negligible and lower than the MLP. The R^2 criterion for EE output is lower than other outputs, and the error measures for EE for both MLP and NN are greater than those of other outputs.

The RSM-generated data through MLP and NN functions, when compared to real optimizer data, have residuals whose normalized percentage is exhibited in Fig. 16. The range of residual variation for MLP (±4 %) is more than the normalized residuals for NN (−0.5–0.75 %). The LCOE and H_2 production show a considerable residual, particularly in initial designs for MLP. Regarding the NN function, however, the more deviation occurs for LCOE and LCOH, and the residuals for IDs after 120 are very close to zero, showing the stability of the virtual design system.

The generated data from the MLP type of RSM modeling is used for 3D evaluation of EE as a function of the electrolyzer input and battery discharge (Fig. 17). The results can successfully capture the impact of input variables on the selected output. Increasing the electrolyzer input reduces the excess electricity because the received electricity power is used to generate the green hydrogen, and the excess hydrogen is stored in the HTank. However, the battery discharge amount shows a direct relation with the excess electricity since the stored energy is released and makes surplus electric energy. Additionally, the electrolyzer's impact on EE is particularly higher than the battery, and it can reduce the EE from over 120.0 kW–40.0 kW if the electrolyzer operates in its full 100.0 kW capacity.

The 2D plot representation of the co-variation of LCOE, EE, and hydrogen production based on MOGT-NN virtual design data is shown in Fig. 18. The hydrogen production is considered in three scales of 0.828, 1.29, and 1.8 kg/h, and four levels of excess electricity are selected as 45.46, 77.56, 113.9, and 151.2 kW. Along with a higher hydrogen production rate, the LCOE is lower compared to lower hydrogen production. It can be confirmed that around EE = 60 kW, there is a minimum LCOE. To decrease the cost of energy for the proposed hybrid system, the hydrogen production must be increased, indicating the role of hydrogen storage in the economic feasibility of the cogeneration system based on hydrogen-to-power and Power-to-hydrogen. For a constant high EE = 151.2 kW, there is a great resonance of LCOE when hydrogen production increases, while for lower EEs, LCOE tends to decrease gradually with hydrogen production. When the system produces a large excess of electricity, the system is exposed to instabilities.

6. Limitations and future work

However, the study acknowledges certain limitations. The reliance on static optimization parameters limits the system's responsiveness to dynamic environmental and operational changes. Furthermore, the scalability of the proposed system to regions with differing resource profiles or larger-scale applications remains to be fully explored. Challenges also exist in terms of computational efficiency, particularly when addressing real-time operational adjustments or expanding the system's complexity. Another limitation is that devices like batteries and electrolyzers exhibit operational delays. Future studies could consider their dynamic behavior, such as startup/shutdown time and response speed.

It is recognized that real-world conditions entail a more variable electrolyzer efficiency, hydrogen leakage, and degradation under extreme Arctic settings. These effects, along with spatial and temporal fluctuations in renewable resources, necessitate the integration of future probabilistic models. Adaptive data-driven modeling, resilience incorporation, and stochastic simulations are the limits and boundaries of the current study to improve robustness in future work.

The future version of this work can be extended to include a full lifecycle analysis (LCA) and carbon footprint analysis of various alternative hybrid systems, from renewable component manufacturing to hydrogen infrastructure, battery degradation, and the end-of-life and disposal stages, thereby supporting a sustainability benchmark.

7. Conclusion

This study successfully demonstrated the feasibility and significant advantages of an optimized hybrid off-grid energy system integrating hydrokinetic, wind, and hydrogen-electricity conversion technologies for remote and demanding environments like the Arctic. Through a two-tier optimization framework, an initial cost-effective system architecture was identified, followed by advanced internal optimizations using Multi-Objective Game Theory (MOGT) and HYBRID algorithms. These optimizations substantially improved system performance, leading to a significant reduction in Net Present Cost (NPC) to as low as $666K and Levelized Cost of Hydrogen (LCOH) to $13.74/kg with MOGT. The innovative incorporation of AI-driven meta-models, specifically Response Surface Methodology (RSM) and Neural Networks (NN), as virtual optimizers proved crucial for efficiently exploring complex design spaces and fine-tuning energy flow strategies. This approach not only facilitated rapid convergence to optimal solutions but also effectively managed the intermittency of renewable sources, ensuring a stable power supply for diverse applications, including cruise ship cold ironing, FCHEV refueling, and residential heating.

The findings underscore the immense potential of such intelligent, integrated renewable energy systems to provide cost-effective, reliable, and sustainable power, offering a type of solution for addressing critical energy challenges in other remote and resource-constrained regions globally.

CRediT authorship contribution statement

Hadi Taghavifar: Writing – review & editing, Writing – original draft, Visualization, Validation, Methodology, Investigation, Data curation, Conceptualization. **Chiara Bordin:** Writing – review & editing, Writing – original draft, Methodology, Formal analysis. **Hao Chen:** Writing – review & editing, Writing – original draft, Investigation, Data curation. **Anthony Paul Roskilly:** Writing – review & editing, Supervision, Resources.

Declaration of competing interest

The authors declare that they have no known competing financial interests or personal relationships that could have appeared to influence the work reported in this paper.

Acknowledgements

The project has received funding from the UArctic 2022 Project with Project No. 580512112.

Appendix

Table A1
Ranked system architecture with main output characteristics

	LCOH ($/kg)	NPC ($)	COE ($)	Architecture	Renewable fraction	Excess electricity	NOx (kg/yr)
Case 1	20.4	1104029	1.4	1-0-2-1	93.70 %	55.30 %	0
Case 2	19.7	1182726	1.5	2-50kW-0-1	93.90 %	69.30 %	0.00893
Case 3	20.5	1211031	1.53	2-20kW-1-1	93.80 %	67.20 %	0.00789
Case 4	25.9	1404238	1.78	3-0-3-0	93.70 %	76 %	0

References

[1] D.J. Dankel, W.J. Boonstra, M. Bjørkan, J.L. Fuller, L. Iversen, S. Eskeland Schütz, B. Staal, G.I. van der Meeren, I. van Putten, Localizing the sustainable development goals for marine and coastal management in Norway: a venture overdue. InHuman-Nature Interactions: Exploring Nature's Values Across Landscapes, Springer International Publishing, Cham, 2022 Jul 1, pp. 343–359.

[2] P. Ortega-Arriaga, O. Babacan, J. Nelson, A. Gambhir, Grid versus off-grid electricity access options: a review on the economic and environmental impacts, Renew. Sustain. Energy Rev. 143 (2021 Jun 1) 110864.

[3] Y. Mohammadi, A. Palstev, B. Polajzer, S.M. Miraftabzadeh, D. Khodadad, Investigating winter temperatures in Sweden and Norway: potential relationships with climatic indices and effects on electrical power and energy systems, Energies 16 (14) (2023 Jul 24) 5575.

[4] E. Moe, S.T. Hansen, E.H. Kjær, Why Norway as a Green Battery for Europe is Still to Happen, and Probably will Not. New Challenges and Solutions for Renewable Energy: Japan, East Asia and Northern Europe, 2021, pp. 281–317.

[5] Forfang SA, Stange KK. A Mixed Methods Approach to Assessing Future Sustainable Energy Solutions in Norway (master's Thesis, NTNU).

[6] N.N. Bakar, N. Bazmohammadi, J.C. Vasquez, J.M. Guerrero, Electrification of onshore power systems in maritime transportation towards decarbonization of ports: a review of the cold ironing technology, Renew. Sustain. Energy Rev. 178 (2023 May 1) 113243.

[7] I.R. Dahl, B.W. Tveiten, E. Cowan, The case for policy in developing offshore wind: lessons from Norway, Energies 15 (4) (2022 Feb 21) 1569.

[8] S. Mishra, E. Ören, C. Bordin, F. Wen, I. Palu, Features extraction of wind ramp events from a virtual wind park, Energy Rep. 6 (2020) 237–249.

[9] O. Gaidai, A. Ashraf, Y. Cao, Y. Zhu, J. Sheng, H. Li, Z. Liu, Multivariate ocean waves dynamics in North Sea and Norwegian Sea by Gaidai reliability method, Energy Rep. 12 (2024 Dec 1) 2346–2355.

[10] B. Emmel, B. Bjørkvik, T.L. Frøyen, P. Cerasi, A. Stroisz, Evaluating the hydrogen storage potential of shut down oil and gas fields along the Norwegian continental shelf, Int. J. Hydrogen Energy 48 (63) (2023 Jul 26) 24385–24400.

[11] C.S. Cheng, Does time matter? A multi-level assessment of delayed energy transitions and hydrogen pathways in Norway, Energy Res. Social Sci. 100 (2023 Jun 1) 103069.

[12] A. Rolán, P. Manteca, R. Oktar, P. Siano, Integration of cold ironing and renewable sources in the barcelona smart port, IEEE Trans. Ind. Appl. 55 (6) (2019 Apr 11) 7198–7206.

[13] O. Yuksel, M. Bayraktar, A. Seyhan, Environmental and economic analysis of cold ironing using renewable hybrid systems, Clean Technol. Environ. Policy 6 (2024 Nov) 1–29.

[14] N. Sifakis, E. Vichos, A. Smaragdakis, E. Zoulias, T. Tsoutsos, Introducing the cold-ironing technique and a hydrogen-based hybrid renewable energy system into ports, Int. J. Energy Res. 46 (14) (2022 Nov) 20303–20323.

[15] S.H. Dolatabadi, A.I. Ölçer, S. Vakili, The application of hybrid energy system (hydrogen fuel cell, wind, and solar) in shipping, Renew. Energy Focus 46 (2023 Sep 1) 197–206.

[16] D. Colarossi, P. Principi, Optimal sizing of a photovoltaic/energy storage/cold ironing system: life cycle cost approach and environmental analysis, Energy Convers. Manag. 291 (2023 Sep 1) 117255.

[17] H. Togun, H.S. Aljibori, A.M. Abed, N. Biswas, M.T. Alshamkhani, H. Niyas, H. I. Mohammed, F.L. Rashid, D. Paul, A review on recent advances on improving fuel economy and performance of a fuel cell hybrid electric vehicle, Int. J. Hydrogen Energy 89 (2024 Nov 4) 22–47.

[18] P. Cheekatamarla, V. Sharma, B. Shen, Sustainable energy solutions for thermal load in buildings—role of heat pumps, solar thermal, and hydrogen-based cogeneration systems, J. Eng. Sustain. Build. Cities 2 (3) (2021 Aug 1) 034501.

[19] D. Trapani, P. Marocco, D. Ferrero, K.B. Lindberg, K. Sundseth, M. Santarelli, The potential of hydrogen-battery storage systems for a sustainable renewable-based electrification of remote islands in Norway, J. Energy Storage 75 (2024 Jan 1) 109482.

[20] S. Damman, E. Sandberg, E. Rosenberg, P. Pisciella, I. Graabak, A hybrid perspective on energy transition pathways: is hydrogen the key for Norway? Energy Res. Social Sci. 78 (2021 Aug 1) 102116.

[21] Ø. Ulleberg, T. Nakken, A. Ete, The wind/hydrogen demonstration system at Utsira in Norway: evaluation of system performance using operational data and updated hydrogen energy system modeling tools, Int. J. Hydrogen Energy 35 (5) (2010 Mar 1) 1841–1852.

[22] T. Kakken, U. Hafseld, E. Fjermestad Hagen, K. Schoffel, I. Hexeberg, The Utsira wind-hydrogen system-lessons Learned, 2005.

[23] Q. Hassan, S. Algburi, A.Z. Sameen, M. Jaszczur, H.M. Salman, Hydrogen as an energy carrier: properties, storage methods, challenges, and future implications, Environ. Syst. Dec. 44 (2) (2024 Jun) 327–350.

[24] M. Kamran, M. Turzyński, Exploring hydrogen energy systems: a comprehensive review of technologies, applications, prevailing trends, and associated challenges, J. Energy Storage 96 (2024 Aug 15) 112601.

[25] H. Ishaq, I. Dincer, C. Crawford, A review on hydrogen production and utilization: challenges and opportunities, Int. J. Hydrogen Energy 47 (62) (2022 Jul 22) 26238–26264.

[26] M. Younas, S. Shafique, A. Hafeez, F. Javed, F. Rehman, An overview of hydrogen production: current status, potential, and challenges, Fuel 316 (2022 May 15) 123317.

[27] L. Mortensen, A.M. Hansen, A. Shestakov, How three key factors are driving and challenging implementation of renewable energy systems in remote Arctic communities, Polar Geogr. 40 (3) (2017 Jul 3) 163–185.

[28] M. de Witt, H. Stefánsson, Á. Valfells, J.N. Larsen, Energy resources and electricity generation in Arctic areas, Renew. Energy 169 (2021 May 1) 144–156.

[29] J. Malito, E. Eidam, J. Nienhuis, Increasing wave energy moves Arctic continental shelves toward a new future, J. Geophys. Res.: Oceans 127 (9) (2022 Sep) e2021JC018374.

[30] A.A. Kolomeytseva, A.K. Krivorotov, Arctic energy sector under low-carbon transition. Inthe Handbook of the Arctic: a Broad and Comprehensive Overview, Springer Nature Singapore, Singapore, 2022 Sep 14, pp. 269–299.

[31] A. Hossain, M.A. Al Mamun, K. Hossain, H.B. Rahman, H.M. Al-Jawahry, M. M. Melon, AI-Driven optimization and management of decentralized renewable energy grids, Nanotechnol. Percept. 18 (2024 Aug) 76–97.

[32] P. Marocco, R. Novo, A. Lanzini, G. Mattiazzo, M. Santarelli, Towards 100% renewable energy systems: the role of hydrogen and batteries, J. Energy Storage 57 (2023) 106306.

[33] O.F. Eikeland, H. Apostoleris, S. Santos, K. Ingebrigtsen, T. Boström, M. Chiesa, Rethinking the role of solar energy under location specific constraints, Energy 211 (2020) 118838.

[34] T. Sikveland, E. Wangen, Interviewees, Project Manager and Electrical Manager at Port of Kristiansand, 30 September 2019 [Interview].

[35] Havn Tromsø, Statistikk [Online]. Available: https://www.tromso.havn.no/om-oss/om-oss/statistikk/, 2019.

[36] A. Al-Sharafi, A.A. Alsubaie, A.S. Al-Buraiki, Green hydrogen, electricity, and heat multigeneration via using solar, wind and hybrid RE systems: comprehensive case studies in Arabian Peninsula Countries, Int. J. Hydrogen Energy 107 (2025) 597–617.

[37] Wind and wave data. https://www.barentswatch.no/bolgevarsel/.

[38] https://ocean.met.no/.

[39] J. Koponen, Review of Water Electrolysis Technologies and Design of Renewable Hydrogen Production Systems, 2015.

[40] A. Ursua, L.M. Gandia, P. Sanchis, Hydrogen production from water electrolysis: current status and future trends, Proc. IEEE 100 (2) (2011) 410–426.

[41] S. Diaf, D. Diaf, M. Belhamel, M. Haddadi, A. Louche, A methodology for optimal sizing of autonomous hybrid PV/wind system, Energy Policy 35 (11) (2007) 5708–5718.

[42] L.I. Lago, F.L. Ponta, L. Chen, Advances and trends in hydrokinetic turbine systems, Energy Sustain. Develop. 14 (4) (2010) 287–296.

[43] A.G. Olabi (Ed.), Renewable Energy-Volume 1: Solar, Wind, and Hydropower: Definitions, Developments, Applications, Case Studies, and Modelling and Simulation, Elsevier, 2023.

[44] A. Al-Sharafi, A.Z. Sahin, T. Ayar, B.S. Yilbas, Techno-economic analysis and optimization of solar and wind energy systems for power generation and hydrogen production in Saudi Arabia, Renew. Sustain. Energy Rev. 69 (2017) 33–49.

[45] P.T. Kapen, B.A.M. Nouadje, V. Chegnimonhan, G. Tchuen, R. Tchinda, Techno-economic feasibility of a PV/battery/fuel cell/electrolyzer/biogas hybrid system for energy and hydrogen production in the far north region of Cameroon by using HOMER pro, Energy Strategy Rev. 44 (2022) 100988.

[46] R.A. Dandekar, Performance improvement of restricted pairing algorithm for Latin hypercube sampling, in: ASA Summer Conference, 1993.

[47] D.M. Kreps, Nash equilibrium, in: Game Theory, Palgrave Macmillan UK, London, 1989, pp. 167–177.
[48] M.T. Hagan, M.B. Menhaj, Training feedforward networks with the Marquardt Algorithm, IEEE Trans. Neural Network. 5 (6) (1994).
[49] D. Nguyen, B. Widrow, Improving the learning speed of 2-Layer neural networks by choosing initial values of the adaptive weights, Proc. IJCNN 3 (1990) 21–26.

Abbreviations

AI: Artificial Intelligence
CAPEX: Capital Expenditure
CHP: Combined Heat and Power
COE: Cost of Energy
DSS: Decision Support Systems
DOE: Design of Experiment
EE: Excess Electricity
FC: Fuel Cell
FCEV: Fuel-Cell Electric Vehicle
FCHEV: Fuel-Cell Hybrid Electric Vehicle
GA: Genetic Algorithm
HK: Hydrokinetic
HKT: Hydrokinetic Turbine
HHV: High Heating Value
HRES: Hybrid Renewable Energy System
HTank: Hydrogen Tank
HYBRID: Hybrid Optimization Algorithm
IQR: Interquartile Range
LHMC: Latin Hypercube-Monte Carlo
LHS: Latin Hypercube Sampling
LHV: Low Heating Value
LCOE: Levelized Cost of Energy
LCOH: Levelized Cost of Hydrogen
MOGT: Multi-Objective Game Theory
MSE: Mean Squared Error
MAE: Mean Absolute Error
MLP: Multi-Layer Perceptron
NN: Neural Network
NPC: Net Present Cost
OPEX: Operational Expenditure
PEM: Proton Exchange Membrane
PL:: Load Power
R2: Coefficient of Determination
RE: Renewable Energy
RSM: Response Surface Methodology
SQP: Sequential Quadratic Programming
WT: Wind Turbine